Cell Reports

Article

GAGE mediates radio resistance in cervical cancers via the regulation of chromatin accessibility

Graphical abstract

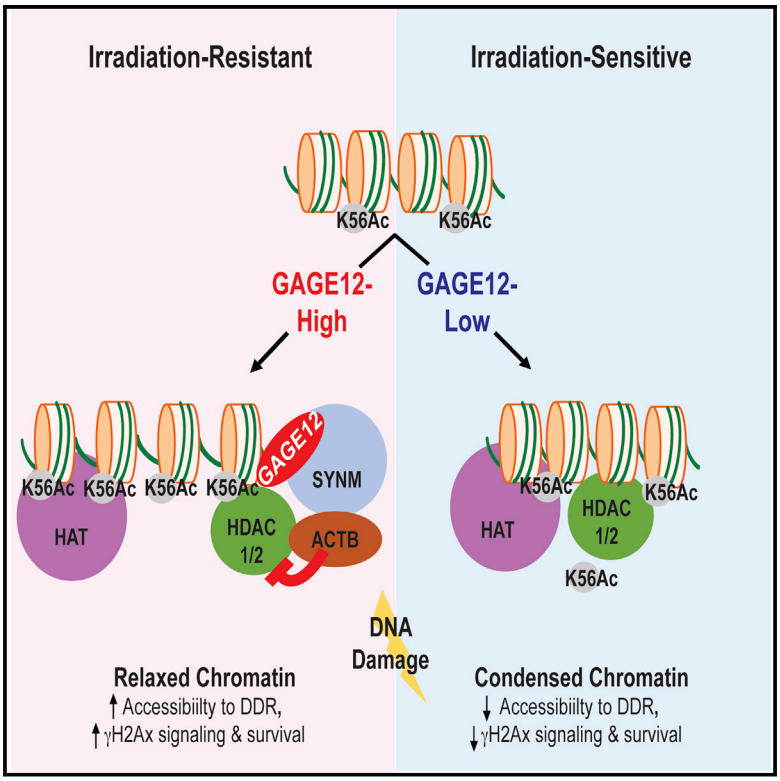

Highlights

- GAGE is expressed at higher levels in radio-resistant cervical cancer
- Only the GAGE12 protein variant contributes to the resistant phenotype
- GAGE12 is localized to the chromatin via its interaction with synemin (SYNM)
- Chromatin-bound GAGE12 mediates HDAC1/2-ACTB association to inhibit H3K56 deacetylation

Authors

Dawn Sijin Nin, Caryn Wujanto, Tuan Zea Tan, ..., Wei Wu, Bok Ai Choo, Lih-Wen Deng

Correspondence

bchnsda@nus.edu.sg (D.S.N.), bchdlw@nus.edu.sg (L.-W.D.)

In brief

The cancer/testis (CT) antigen GAGE is expressed in several cancers. However, the molecular intricacies of how GAGE functions within the cell remains poorly defined. Nin et al. describe a role for GAGE in altering chromatin accessibility, leading to more efficient DNA repair, contributing to the radio-resistant phenotype in cervical cancer.

Nin et al., 2021, Cell Reports *36*, 109621
August 31, 2021 © 2021 The Author(s).
https://doi.org/10.1016/j.celrep.2021.109621

CellPress

Cell Reports

CellPress
OPEN ACCESS

Article

GAGE mediates radio resistance in cervical cancers via the regulation of chromatin accessibility

Dawn Sijin Nin,[1,11,*] Caryn Wujanto,[2,5] Tuan Zea Tan,[3] Diana Lim,[4,5] J. Mirjam. A. Damen,[6] Kuan-Yi Wu,[7] Ziyu Melvin Dai,[1] Zheng-Wei Lee,[1] Shabana Binte Idres,[1] Yiat Horng Leong,[2,5] Sudhakar Jha,[1,3,5,8,11] Joseph Soon-Yau Ng,[5,9] Jeffrey J.H. Low,[5,9] Shih-Chung Chang,[7] David Shao Peng Tan,[3,5,10,11] Wei Wu,[6] Bok Ai Choo,[2,5] and Lih-Wen Deng[1,5,11,12,13,*]

[1]Department of Biochemistry, Yong Loo Lin School of Medicine (YLLSOM), National University of Singapore (NUS), Singapore 117596, Singapore
[2]Department of Radiation Oncology, National University Hospital (NUH), Singapore 119074, Singapore
[3]Cancer Science Institute of Singapore, NUS, Singapore 117599, Singapore
[4]Department of Pathology, NUH, Singapore 119074, Singapore
[5]National University Cancer Institute, Singapore National University Health System (NUHS), Singapore 119074, Singapore
[6]Biomolecular Mass Spectrometry and Proteomics, Bijvoet Center for Biomolecular Research and Utrecht Institute for Pharmaceutical Sciences, Utrecht University, Padualaan 8, 3584 CH Utrecht , the Netherlands
[7]Department of Biochemical Science and Technology, College of Life Science, National Taiwan University, Taipei, Taiwan
[8]Department of Physiological Sciences, College of Veterinary Medicine, Oklahoma State University, Stillwater, OK, USA
[9]Department of Obstetrics and Gynecology, YLLSOM, NUS, Singapore 119228, Singapore
[10]Department of Hematology-Oncology, NUHS, Singapore 119228, Singapore
[11]NUS Center for Cancer Research, YLLSOM, NUS, Singapore 117599, Singapore
[12]NUS Graduate School - Integrative Sciences and Engineering Programme, NUS, Singapore 119077, Singapore
[13]Lead contact
*Correspondence: bchnsda@nus.edu.sg (D.S.N.), bchdlw@nus.edu.sg (L.-W.D.)
https://doi.org/10.1016/j.celrep.2021.109621

SUMMARY

Radiotherapy (RT) resistance is a major cause of treatment failure in cancers that use definitive RT as their primary treatment modality. This study identifies the cancer/testis (CT) antigen G antigen (GAGE) as a mediator of radio resistance in cervical cancers. Elevated GAGE expression positively associates with *de novo* RT resistance in clinical samples. GAGE, specifically the GAGE12 protein variant, confers RT resistance through synemin-dependent chromatin localization, promoting the association of histone deacetylase 1/2 (HDAC1/2) to its inhibitor actin. This cumulates to elevated histone 3 lysine 56 acetylation (H3K56Ac) levels, increased chromatin accessibility, and improved DNA repair efficiency. Molecular or pharmacological disruption of the GAGE-associated complex restores radiosensitivity. Molecularly, this study demonstrates the role of GAGE in the regulation of chromatin dynamics. Clinically, this study puts forward the utility of GAGE as a pre-screening biomarker to identify poor responders at initial diagnosis and the therapeutic potential of agents that target GAGE and its associated complex in combination with radiotherapy to improve outcomes.

INTRODUCTION

Radiotherapy (RT) is an integral component of cancer treatment, and ~50% of patients with cancer will undergo RT during treatment (Baskar et al., 2012). Definitive RT is a primary treatment modality in several cancers, including locally advanced cervical cancer (CC) (Cho and Chun, 2018). The current recommendation for non-surgical definitive treatment of locally advanced CC includes external beam radiotherapy (EBRT) (1.8 Gy × 20–28 daily fractions) given concurrently with platinum-based chemotherapy. This is followed by three to five fractions of high-dose-rate brachytherapy or one to two fractions of low-dose-rate brachytherapy (Banerjee and Kamrava, 2014; Lea and Lin, 2012). However, distant treatment failure still occurs in up to 30% of patients and is attributed to the presence of a subpopulation of radio-resistant cells (Moreno-Acosta et al., 2012). Clinical and molecular studies have shown that certain intrinsic cellular factors may determine how well tumor cells respond and adapt to RT (Rogers et al., 2000; West et al., 1995). Identifying these molecular factors in patients with CC may permit the early prediction of treatment outcomes and improve radiation-induced cancer cell death through the tailoring of RT dose or via the utilization of selective inhibitors of pathways controlled by these factors.

Cancer/testis (CT) antigens are a category of tumor antigens whose expression is restricted to germ cells and tumor cells and absent in somatic cells (Scanlan et al., 2004; Simpson et al., 2005) first identified by autologous genotyping (Coulie

This is an open access article under the CC BY-NC-ND license (http://creativecommons.org/licenses/by-nc-nd/4.0/).

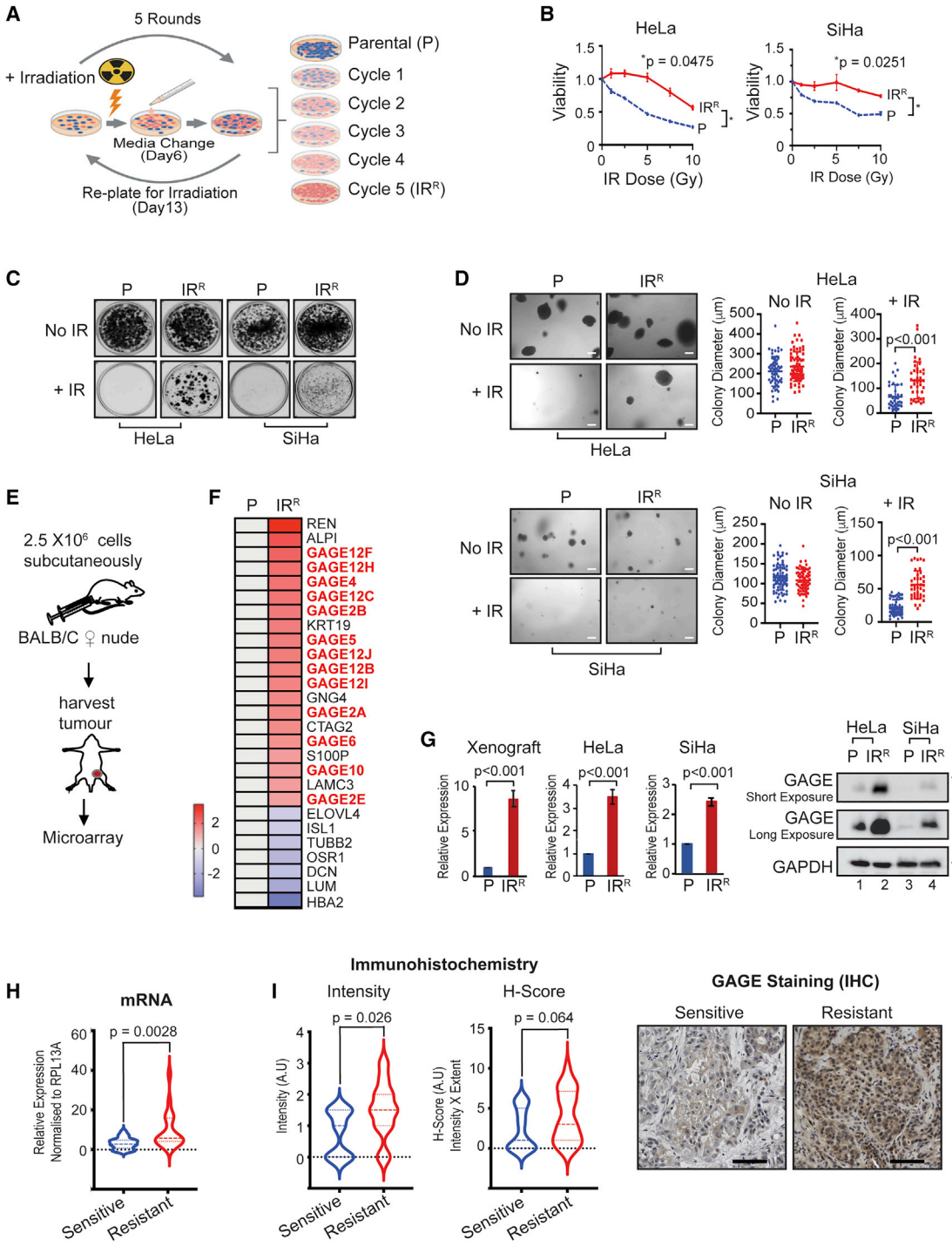

Figure 1. Generation of IR-resistant lines and identification of GAGE

(A) Workflow for the generation of IR-resistant cell lines.

(B) Viability of parental (P) versus IR-resistant (IR^R) cells after γ-irradiation measured 3 days post-treatment. Mean ± SD of 3 biological replicates is represented (t test).

(C) 2D long-term viability of P versus IR^R HeLa and SiHa cells after γ-irradiation measured 14 days post-treatment. Data are representative of 3 biological replicates.

(D) 3D anchorage-independent viability of P versus IR^R HeLa and SiHa cells after γ-irradiation measured 21 days post-treatment and quantitation of colony size. Scale bar, 100 μm. Colony diameters of >50 colonies from 3 biological replicates are represented (t test; mean ± SD).

(E) Workflow for the generation of P and IR^R HeLa xenograft tumors.

(legend continued on next page)

et al., 1993). With the advent of high-throughput PCR and sequencing techniques, there has been a rapid expansion of the number of CT antigens being identified (Boël et al., 1995; Chen et al., 2005; De Backer et al., 1999; Hofmann et al., 2008; da Silva et al., 2017; Liu et al., 2013; Taguchi et al., 2014). However, the functions of many of these genes in cancer pathogenesis remain to be elucidated. The CT antigen, G antigen (GAGE), consists of a group of small acidic proteins with a high degree of sequence homology (Gjerstorff and Ditzel, 2008). The *GAGE* gene locus resides on the human X chromosome and includes four contigs (GenBank: AF235097, BX649339, AC142497, and AC142496). The locus consists of sixteen *GAGE* genes enclosed in an equal number of 9.5 Kbps tandem repeats (Gjerstorff and Ditzel, 2008). Unlike its more well-known counterparts, the melanoma-associated antigen (MAGE) and the New York esophageal squamous cell carcinoma 1 (NY-ESO-1), the role of GAGE in cancer progression is not as well explored, despite its frequent occurrence in malignant melanomas and lung cancer (De Backer et al., 1999; Eichmüller et al., 2002). Currently, apart from its anti-apoptotic role (Cilensek et al., 2002) and contribution to gastric metastasis (Lee et al., 2015; Shi et al., 2019), the function of this family of proteins has been poorly defined.

Histone modifications have essential functions in the cellular environment. The homeostatic balance between acetylation and deacetylation, as well as methylation versus demethylation, plays critical roles in cellular maintenance and response to intra- and extracellular stresses. Further, their influence on chromatin structure is also essential in determining cellular responses to DNA damage. On this front, histone acetylation is critical for creating a decondensed chromatin structure such that repair proteins can access the site of damage (Williamson et al., 2012), enabling proper DNA repair to occur.

In this study, we found that elevated expression of the CT antigen GAGE is involved in the radio-resistant phenotype and could be an early predictor of unfavorable outcomes in patients with CC. Specifically, only the GAGE12 protein variant encoded mainly by the GAGE12 family of mRNAs confers irradiation (IR) resistance to CC cells. We also showed that GAGE12-mediated IR resistance was attributed partly to its ability to create a more ''open'' chromatin structure through the elevation of histone 3 lysine 56 acetylation (H3K56Ac), which could increase DNA repair efficiency. GAGE12's ability to mediate H3K56Ac is attributed to its chromatin localization as a result of its interaction with the intermediate filament synemin (SYNM). This GAGE12-SYNM interaction promotes the association of histone deacetylase 1/2 (HDAC1/2) to its inhibitor actin at specific sites on the chromatin, hindering HDAC1/2's capacity to deacetylate H3K56 at these sites. Essentially, our study links the CT antigen GAGE to the regulation of chromatin dynamics and highlights the potential applications of GAGE as a molecular marker for the early prediction of RT response and a molecular target in CC.

RESULTS

Establishment of IR-resistant CC cell lines

To identify potential molecular markers for RT resistance, we generated IR-resistant CC cell line models of HeLa (HPV18+) and SiHa (HPV16+) by employing a method previously established by Kubo et al. (1982; Figure 1A). HeLa IR-resistant (HeLa IR^R) and SiHa IR-resistant (SiHa-IR^R) cell lines were established with repeated IR and selection of surviving cells for five cycles. Morphologically, IR^R cell lines were indistinguishable from their parental (P) counterparts in 2D cultures but possessed slightly faster growth rates than parental cell lines (Figures S1A and S1B). Interestingly, when cultured in tumor-initiating media (TIM) in an anchorage-independent condition, IR^R cells from both HeLa and SiHa cell lines seemed to form larger tumor spheres than their parental counterparts (Figure S1C). Despite being morphologically similar, IR^R HeLa and SiHa cell lines possess IR resistance in both 2D short-term and long-term survival assays (Figures 1B and 1C) as well as in 3D-anchorage-independent conditions (Figures 1D and S1D).

Identification of GAGE upregulation in IR-resistant cells

IR resistance is the leading cause of treatment failure in CC and is often attributed to variations in genetic factors between the IR-sensitive and resistant cell populations. Potential genetic markers whose expressions correlated with IR resistance were identified using microarray analysis of excised xenograft tumors generated from HeLa P and IR^R cell lines (Figure 1E). Intriguingly, out of the 20 most upregulated genes, we noticed that 13 of them belong to the cancer/testis antigen, GAGE family (Figure 1F). We further validated the increased expression of GAGE in our xenograft mouse and cell line models at both the mRNA and protein levels (Figure 1G). These findings suggest that the GAGE family of proteins may have a role in conferring IR resistance to CC cells.

To strengthen our clinical correlation studies, we analyzed archival formalin-fixed paraffin-embedded (FFPE) clinical samples obtained during initial diagnosis from patients with CC, with at least 2-year follow-up data after treatment from the National University Hospital in Singapore. All patients underwent definitive EBRT with concurrent weekly platinum-based chemotherapy followed by brachytherapy. Here, we defined patients with local and/or distant recurrence as resistant (n = 20) and those in remission at their last follow-up as sensitive (n = 23). We found that patients in the resistant group had higher average levels of GAGE expression both at mRNA and protein levels (Figures 1H and 1I) in their pre-treatment biopsy samples. These

(F) Heatmap depicting the top 20 most upregulated and the 7 most downregulated genes in microarray analysis. Log2FC of expression compared to P is shown; GAGE genes are highlighted in red.

(G) Validation of increased GAGE mRNA expression in IR^R HeLa xenograft tumors and HeLa and SiHa cells (left panel). Mean ± SD of 3 technical replicates is represented (t test). Increased GAGE protein expression in HeLa and SiHa IR^R lines (right panel) is shown.

(H and I) *GAGE* mRNA expression (H) and protein expression determined by immunohistochemistry (I) in archival FFPE embedded first biopsy samples from patients who completed radiotherapy. Resistant, patients who presented with recurrence and metastasis in subsequent 2-year follow-up (sensitive n = 23 and resistant n = 20). Scale bar, 100 μm (t test; mean ± SEM).

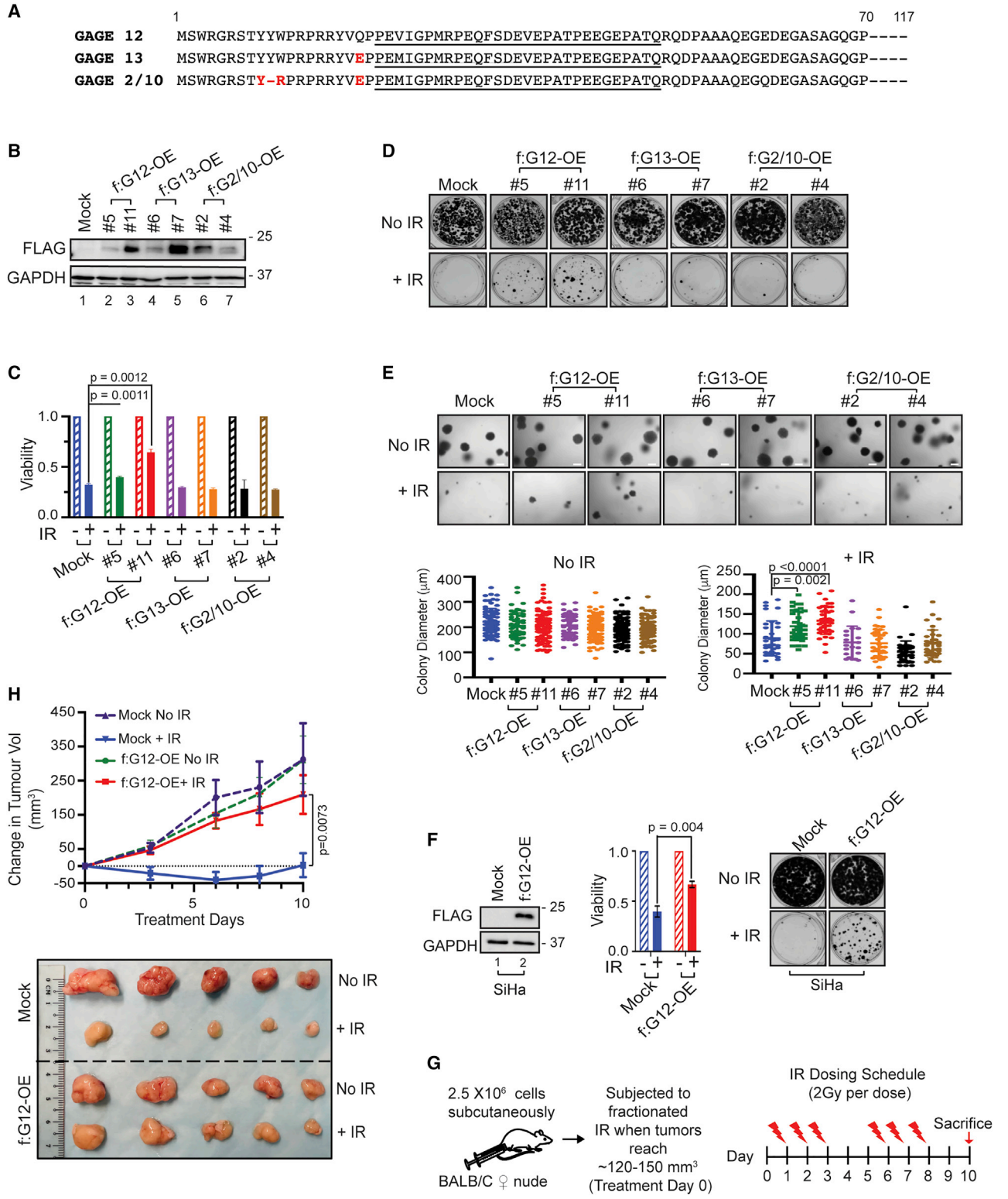

Figure 2. Only GAGE12 confers the IR-resistant phenotype

(A) Protein alignment of GAGE12 and the GAGE13 and GAGE2/10 variants (red, amino acid variations). Underlined sequence is used to raise commercially available antibodies.

(B) Protein expression of FLAG-GAGE12 (f:G12-OE), FLAG-GAGE13 (f:G13-OE), and FLAG-GAGE2/10 (f:G2/10-OE) in HeLa single clones.

(legend continued on next page)

observations indicate that the correlation between increased GAGE expressions with radio resistance is physiologically relevant and is not an artifact of our cell line models.

To clarify the role of GAGE in the radio-resistant phenotype, we next depleted GAGE from radio-sensitive and resistance cells (Figure S2A) to study their effects on radio resistance. However, although we observed a partial reversal of the resistant phenotype in IR^R cell lines (Figures S2B and S2C), we noticed that GAGE-depleted cells could not maintain long-term cell growth and ultimately resulted in decreased cell viability (Figures S2B and S2C). The decrease in cell viability could be due to other previously reported functions of GAGE (Cilensek et al., 2002). Thus, to better elucidate the role of GAGE in conferring radio resistance, we decided to utilize the overexpression system in subsequent studies.

Only the GAGE12 protein variant contributes to the IR-resistant phenotype

The GAGE family of CT antigens are small acidic proteins (117 amino acids) with an almost 98% sequence homology in the coding regions of the mRNA between all identified members (Gjerstorff and Ditzel, 2008). Genes in the GAGE family are grouped according to the following linked variations, 109_111insTAT, 112T>C, and 136C>G, which translates to Y9del, W11R, and Q19E, respectively, in their amino acid sequences. In contrast, mRNA isoforms in each group are differentiated based on their 5′ and 3′ untranslated regions (UTRs). The variations in amino acid sequences mainly occur in the N-terminal region of the GAGE protein and may contribute to functional differences due to amino acid deletions and/or charge modifications. These changes may, in turn, alter protein conformation or interfere with protein-protein interactions. Protein alignment of all GAGE family members available in GenBank shows high sequence homology between all members, with GAGE13 having the Q19E variation and the GAGE2/10 group having the Y9del, W11R, and Q19E variations. However, the majority of the transcripts translate to the unaltered GAGE protein, which, for simplicity of nomenclature, will be called GAGE12 in this study, as the largest number of transcripts that translate to the full unaltered sequence belongs to the GAGE12 family (Figure S2D). The alterations in amino acid sequences found in GAGE13 and GAGE2/10 might contribute to functional differences between GAGE13 or GAGE2/10 and the GAGE12 family of proteins (Figure 2A).

Due to the high sequence homology of all the GAGE proteins, commercially available GAGE antibodies are currently raised using the peptide sequence from amino acids 21–49 (Figure 2A, underlined), which detects all GAGE variants, making it a challenge to study the functional role of different GAGE protein variants endogenously. Therefore, we generated HeLa clones stably expressing the FLAG-tagged GAGE12 (FLAG-GAGE12) protein, which expresses the complete amino acid sequence encoded by most of the GAGE mRNAs (f:G12-OE); the FLAG-GAGE13 protein (f:G13-OE), which has the Q19E variation; and the FLAG-GAGE2/10 protein, which has the Y9del, W11R, and Q19E variations in their protein sequences (f:G2/10-OE; Figure 2B) to investigate functional differences between the protein variants. Interestingly, we found that only HeLa cells expressing the GAGE12 protein showed the most profound IR-resistant phenotype in both 2D (Figures 2C and 2D) and 3D assays (Figures 2E and S3A). GAGE12's ability to confer resistance seems to correlate with protein expression levels. This was demonstrated in long-term viability assays where f:G12-OE no. 11, which expresses a higher level of the GAGE12 protein compared to f:G12-OE no. 5, is more resistant to IR-induced cell death (Figures 2D and 2E). SiHa cells that express FLAG-GAGE12 were also more resistant to IR-induced cell death than their mock-transfected counterparts, suggesting that the ability of GAGE12 to confer the radio-resistant phenotype is not limited to HeLa cells (Figure 2F).

We next generated xenograft mice models of mock or GAGE12 (f:G12-OE)-expressing HeLa cells (Figure S3B). Mice were subjected to fractionated IR at 2 Gy per fraction up to a total of 12 Gy over 10 days (Figure 2G). We observed that f:G12-OE tumors were more resistant to the tumor-suppressive effects of IR, and its tumor size continually enlarged during treatment. In contrast, mock tumors displayed halted growth during treatment (Figure 2H). We also noted that IR-treated mice were lighter in weight post-IR compared to their non-treated counterparts, an observation consistent with the known side effects of RT (Figure S3C).

Next, we evaluated the potential prognostic value of different GAGE mRNA isoforms. Available GAGE variant expression data in the TCGA database was interrogated and correlated to the best radiotherapy response. Of note, pan-cancer samples with GAGE transcripts detected in The Cancer Genome Atlas (TCGA) were used, as those with no transcripts detected may be a result of low coverage. Thus, for this analysis, we focused only on the samples with detected GAGE transcripts. Despite this shortfall, we still observed that a larger portion of patients with partial response (PR) and progressive disease (PD) appear to have higher levels of GAGE12 expression compared to those with complete response. This trend was not observed in GAGE2 and GAGE10 (Figure S3D).

As part of the efforts to study the clinical relevance of GAGE levels and RT resistance, a small prospective study was initiated at the Radiation Therapy Centre in the National University

(C) Viability of FLAG-GAGE HeLa single clones after γ-irradiation measured 3 days post-treatment. Mean ± SD of 3 biological replicates is represented (t test).
(D) Long-term colony formation ability of mock versus FLAG-GAGE HeLa single clones after γ-irradiation 14 days post-treatment. Data are representative of 3 biological replicates.
(E) 3D anchorage-independent viability of mock versus FLAG-GAGE HeLa single clones 21 days post-γ-irradiation and quantitation of colony size (bottom panel). Scale bar, 100 μm. Colony diameters of >50 colonies from 3 biological replicates are represented (t test; mean ± SD).
(F) GAGE expression (left panel) and viability of mock versus f:G12-OE SiHa cells in short-term (3 days) viability assays (middle panel) and long-term (14 days) colony formation (right panel) after exposure to γ-irradiation. Data are representative of 3 biological replicates (t test; mean ± SD).
(G) Outline of the IR treatment protocol for FLAG-GAGE12 (f:G12-OE) HeLa xenograft models.
(H) Changes in tumor volume measure every 2 days during the IR treatment. Average volumes ± SEM are represented. Mock ± IR (n = 5 per group) and f:G12-OE ± IR (n = 5 per group; top panel) are shown. Excised tumors post-IR (bottom panel) are shown. Data are representative of 3 independent experiments.

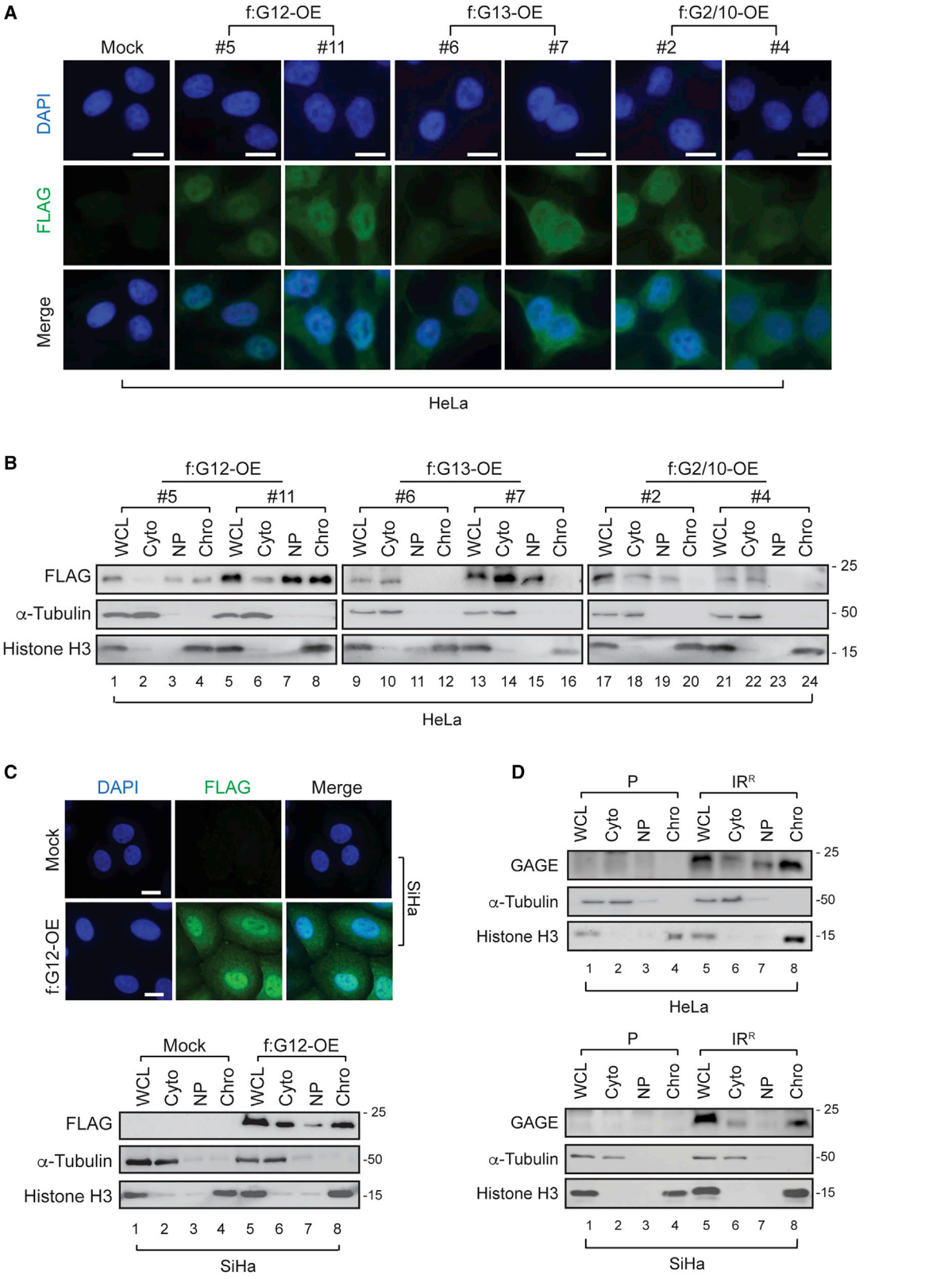

(legend on next page)

Hospital Singapore. Patients diagnosed with locally advanced CC were classified as resistant if their tumors did not reduce by >50% on clinical examination after completing definitive chemo-radiotherapy (CRT). Analysis of GAGE levels in pre-treatment biopsy samples of eight patients who completed treatment revealed that patients with resistant tumors (n = 3) had higher levels of GAGE mRNA compared to those who were sensitive (n = 5; Figure S3E, left panel). Interestingly, in biopsy specimens of residual tumors collected post-treatment from seven of the patients, we observed that five patients had elevated GAGE levels in their post-treatment residual tumors (Figure S3E, right panel). In addition, we also observed increased GAGE12 expression in f:G12-OE tumors that persisted post-IR compared to their unirradiated counterparts (Figure S3B). These observations suggest that elevated GAGE levels in these residual tumors may contribute to their persistence after standard RT.

Intracellular localization of different GAGE proteins determines their ability to confer IR resistance

To better understand how the different GAGE proteins possess varying abilities to modulate CC cell response to IR, we first looked at the localization of the different GAGE proteins in the different clones. Interestingly, although all GAGE variants seem to be expressed in the nucleus when expressed at high levels in immunofluorescence experiments (Figure 3A; f:G12-OE no. 11 versus f:G13-OE no. 7 versus f:G2/10-OE no. 2), only GAGE12 was found to be bound to the chromatin when nuclear proteins were fractioned into proteins eluted by low salt concentration (nucleoplasm fraction [NP]) and those only eluted in the presence of 500 mM NaCl (chromatin-bound fraction [Chro]; Figure 3B). Similarly, chromatin-bound GAGE12 was also found in SiHa cells expressing FLAG-tagged GAGE12 (Figure 3C, bottom panel). Although currently available antibodies against endogenous GAGE are not able to distinguish between the different GAGE protein variants, we still observed endogenous GAGE in the chromatin fraction of HeLa IR^R and SiHa IR^R cells (Figure 3D, lane 8, top and bottom panels).

The intermediate filament SYNM is required for GAGE12 localization in the chromatin fraction

Having observed the important role of GAGE12 chromatin localization in conferring the IR-resistant phenotype, we first considered possible interactors that may bring GAGE12 to the chromatin. Mass spectrometry analysis of FLAG-GAGE12, immunoprecipitated from the chromatin fraction of FLAG-GAGE12 high-expressing HeLa clone (f:G12-OE no. 11), identified several potential binders for GAGE12. Of the possible interactors, SYNM, an intermediate filament, was identified as one of the most enriched proteins co-immunoprecipitated with FLAG-GAGE12 in the chromatin fraction (Figure 4A). We further validated the interaction between GAGE12 and SYNM in both FLAG and SYNM immunoprecipitation experiments performed using the chromatin fraction of f:G12-OE no. 11 cells (Figures 4B and 4C). Similarly, we found GAGE12 and SYNM interactions in the chromatin fraction of f:G12-OE SiHa cells (Figure S4A). Although our current GAGE antibodies were not ideal for immunoprecipitation experiments, we were able to show GAGE interaction with SYNM in the chromatin fraction of HeLa IR^R cells by immunoprecipitating SYNM and probing for GAGE (Figure 4D). Intriguingly, immunoprecipitation of FLAG-tagged GAGE13 and GAGE2/10 proteins from total nuclear extracts (used here due to the lack of chromatin-bound GAGE13 and GAGE2/10) of the respective high-GAGE-expressing clones (f:G13-OE no. 7 and f:G2/10-OE no. 2) revealed that only GAGE12 was able to co-immunoprecipitate SYNM (Figure 4E). This observation is fascinating in that a single mutation in GAGE13 (from neutral glutamine [Q] to a negatively charged glutamic acid [E]) could abolish GAGE interaction with SYNM. SYNM is an intermediate filament that localizes in both peripheral and nuclear regions of glioblastoma cells (Pitre et al., 2012). SYNM is also responsible for sequestering protein phosphatase 2A (PP2A) in the nucleus, preventing PP2A dephosphorylation of Akt in the cytosol (Pitre et al., 2012). Therefore, we hypothesized that GAGE12 interaction with SYNM could be accountable for GAGE12's localization in the chromatin fraction. Indeed, in f:G12-OE cells, although we detect significant expression of GAGE12 in the Chro fraction, knockdown of SYNM in these cells resulted in a considerable reduction of GAGE12 in the NP and Chro fractions (Figure 4F, top panel, lanes 3 and 4 versus 7 and 8) and accumulation of GAGE12 in cytoplasm (Cyto) fraction (Figure 4F, top panel, lane 2 versus 6). A similar phenomenon was observed in HeLa IR^R cells, which expressed higher levels of GAGE (Figure 4F, bottom panel) and in f:G12-OE SiHa cells (Figure S4B), suggesting that SYNM is involved in the localization of GAGE12 in the chromatin fraction. Because chromatin localization of GAGE12 seemed to be important in conferring the IR-resistant phenotype, loss of SYNM and therefore inability of GAGE12 to localize to the chromatin should re-sensitize IR-resistant cells to the cytotoxic effects of IR. Indeed, in both f:G12-OE and IR^R cells, knockdown of SYNM resulted in the loss of the IR-resistant phenotype (Figures 4G and S4C). Taken together, these findings suggest that SYNM is involved in bringing GAGE12 to the chromatin, and this localization of GAGE12 is vital in the observed IR-resistant phenotype.

Expression of GAGE12 is associated with a more open chromatin structure and faster DNA repair dynamics

In our initial immunofluorescence studies into GAGE localization, we consistently observed larger nuclei in DAPI staining of both IR^R

Figure 3. GAGE12 shows preferential chromatin localization

(A) Localization of GAGE isoforms in FLAG-GAGE HeLa single clones analyzed by immunofluorescence. Green, FLAG-GAGE variant; blue, DAPI. Scale bar, 10 μm.

(B) Localization of GAGE protein variants in FLAG-GAGE HeLa single clones after fractionation (WCL, whole cell lysate; Cyto, cytosolic fraction; NP, nucleoplasm fraction; Chro, chromatin fraction).

(C) Localization of GAGE12 protein FLAG-GAGE12 SiHa cells analyzed by immunofluorescence (top panel) and after fractionation (bottom panel). Scale bar, 10 μm.

(D) Localization of GAGE in HeLa (top panel) and SiHa (bottom panel) P and IR^R cells after fractionation.

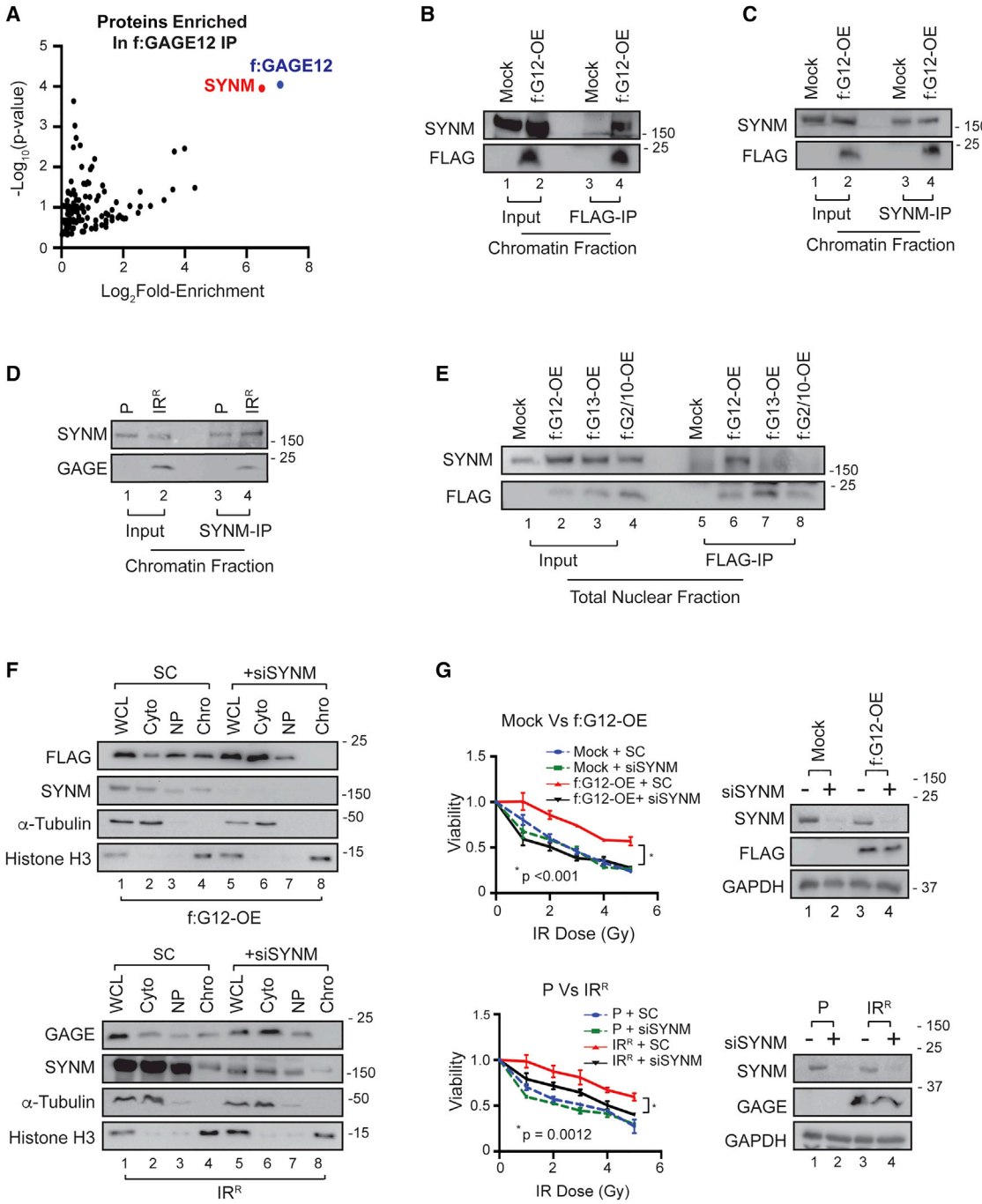

Figure 4. The intermediate filament synemin is required for GAGE12 in the chromatin fraction

(A) Enrichment plot of proteins in the chromatin fractions of mock versus FLAG-GAGE12-OE (f:G12-OE) cells enriched after immunoprecipitation using anti-FLAG antibody. Synemin (SYNM), which is the most enriched, is labeled in red.

(B) Validation of FLAG-GAGE12 and SYNM interaction in the chromatin fractions of mock versus f:G12-OE cells using FLAG as bait in immunoprecipitation.

(C) Validation of FLAG-GAGE12 and SYNM interaction in the chromatin fractions of mock versus f:G12-OE cells using SYNM as bait.

(D) Validation GAGE and SYNM interaction in the chromatin fractions of P versus IR^R HeLa cells using SYNM as bait.

(E) SYNM only interacts with FLAG-GAGE12 in total nuclear fractions of mock versus FLAG-GAGE HeLa single clones using FLAG as bait.

(F) Localization of GAGE after SYNM knockdown. Loss of chromatin localization of f:GAGE12 or endogenous GAGE in f:G12-OE (top panel) and IR^R cells (bottom panel) after SYNM knockdown.

(G) Re-sensitization of f:G12-OE cells and IR^R cells to IR after SYNM knockdown. Viability is measured 3 days post IR. Mean ± SD of 3 biological replicates is represented (t test).

CellPress
OPEN ACCESS

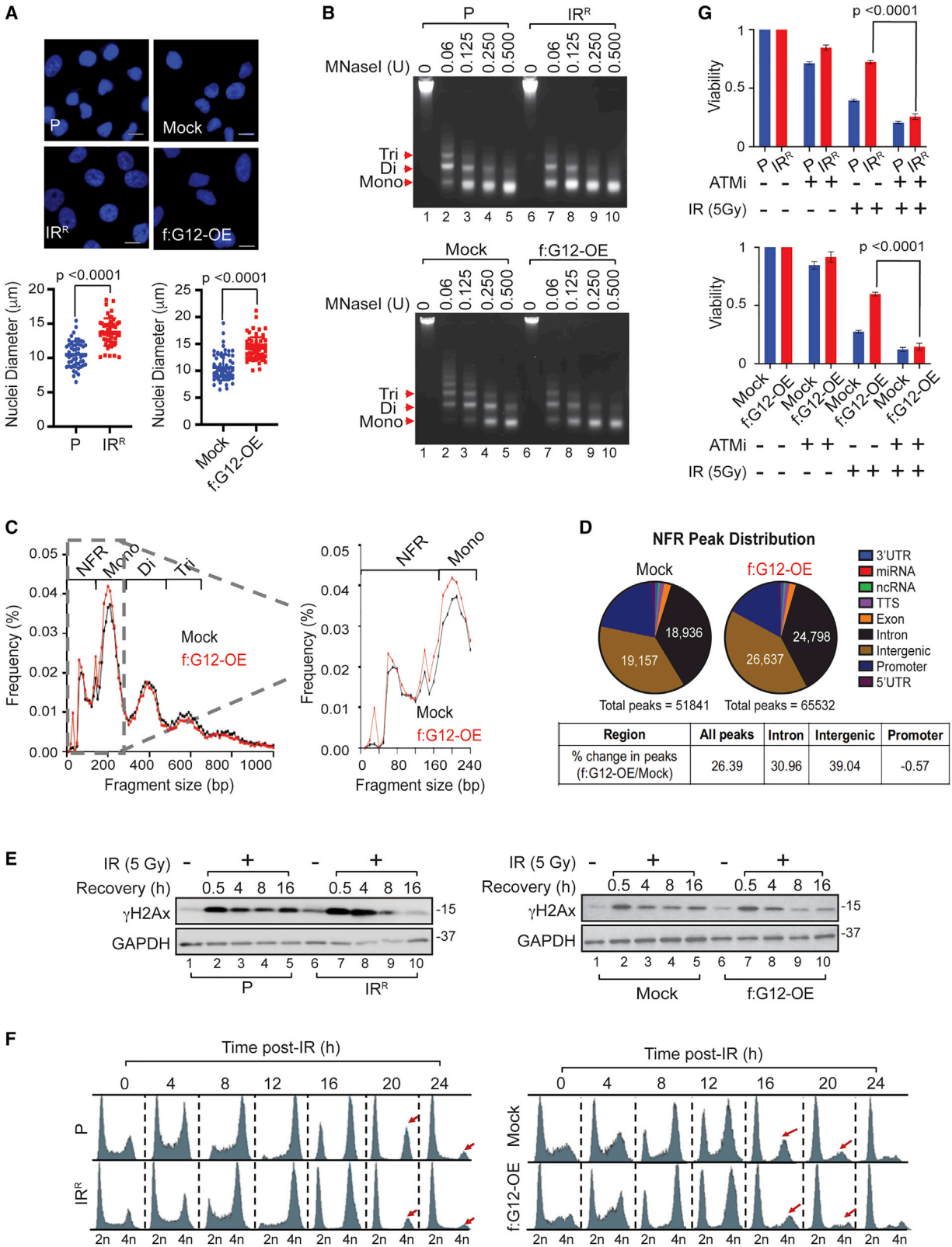

Region	All peaks	Intron	Intergenic	Promoter
% change in peaks (f:G12-OE/Mock)	26.39	30.96	39.04	-0.57

(legend on next page)

cells and cells expressing the GAGE12 variant (f:G12-OE) compared to P and mock-transfected cells (Figure 5A). Larger nuclei are often associated with an increased proportion of cells in the S phase or a more "open" chromatin structure, both of which have been associated with resistance to IR-induced cell death (Floyd et al., 2013; Nicolay et al., 2012). In this instance, we did not find a significant increase in S phase cells in both IR^R and f:G12-OE cells compared to their P and mock counterparts (Figures S5A and S5B). Interestingly, we found that IR-resistant IR^R and f:G12-OE cells had a more open chromatin structure as compared to their IR-sensitive P and mock counterparts. This was evident in micrococcal nuclease I (MNaseI) digestion assay, where IR^R and f:G12-OE cells consistently released more mono-nucleosomes at every concentration of MNaseI used compared to P and mock cells (Figure 5B). Similarly, f:G12-OE SiHa cells also had chromatin that was more accessible to MNaseI digestion although S phase proportion was not significantly different in mock versus f:G12-OE cells (Figures S5C and S5D). In addition, knockdown of GAGE in HeLa P cells resulted in a more condensed chromatin structure with lesser mono-nucleosome released when treated with MNaseI (Figure S5E). We also performed assay of transposase accessible chromatin sequencing (ATAC-seq) in mock and f:G12-OE HeLa cells and found that, consistent with our observations using MNaseI, there was an increase in the number of nucleosome-free and mono-nucleosome peaks detected in f:G12-OE cells compared to their mock counterparts (Figure 5C). Of note, while we observed an overall 26.39% increase in ATAC-seq peaks in the nucleosome-free region (NFR) of f:G12-OE versus mock cells, it was interesting to note that the major increase was in the intron (30.96% relative to mock) and intergenic (39.04% relative to mock) regions (Figure 5D). Together, our data suggest better MNaseI and transposase accessibility in f:G12-OE cells, indicating more accessible chromatin in these cells. In a previous study by Floyd et al. (2013), it was observed that cells with less compact chromatin were more resistant to IR-induced cell death due to their ability to repair DNA lesions at a faster rate as a consequence of better accessibility to DNA damage repair factors. Similarly, we noticed an increased ability to resolve IR-induced DNA lesions in IR-resistant IR^R and f:G12-OE cells, with γH2Ax levels returning to basal levels 8 h post-IR. In comparison, P and mock cells had sustained γH2Ax levels up to 16 h post-IR (Figure 5E). Interestingly, we also observed that, in its native state, there was a slight increase in γH2Ax levels in IR^R and f:G12-OE cells (Figure 5E, lane 1 versus 6, left and right panels), which is also indicative of a more decondensed chromatin structure. Additionally, IR^R and f:G12-OE cells progressed from IR-induced G2 cell cycle arrest faster than P and mock cells (Figure 5F).

Traditionally, exposed DNA is more sensitive to the DNA-damaging effects of IR. However, reports have also suggested that a more open chromatin structure could improve the recruitment of DNA damage repair factors to damage sites and improve DNA repair efficiency (Floyd et al., 2013). In the case of cells expressing elevated GAGE levels, we hypothesized that the ability to repair the inflicted damage outweighs the potentially higher load of damage and treatment with inhibitors of the DNA damage pathway would re-sensitize GAGE-high cells to the cytotoxic effects of IR. Indeed, when treated with a specific inhibitor of ATM (ATMi) KU60019, both GAGE-high IR^R and f: G12-OE cells were now re-sensitized to the cytotoxic effects of IR (Figure 5G). In summary, our data thus far suggest that high GAGE12 expression coupled with its localization to the chromatin is associated with a more open chromatin structure, which consequently leads to an increase in DNA repair efficiency.

GAGE12 modulates H3K56Ac through attenuation of HDAC activity

Histone acetylation transforms chromatin into a more open structure by removing the positive charge on histones, thereby decreasing their interaction with the negatively charged phosphate groups of DNA and by recruiting chromatin modifiers to acetylated sites. We subsequently investigated how GAGE12 may have brought about the observed changes in chromatin structure by probing changes in global acetylation of known histone residues. Intriguingly, of the multiple known histone acetylation marks, we consistently found an increase in the H3K56Ac in both IR^R cells and f:G12-OE cells (Figures 6A and S6A). Other histone acetylation marks did not seem to be largely affected in these cells. To further affirm the relationship between GAGE12 expression and alterations in H3K56Ac, we also performed GAGE knockdown in f:G12-OE cells. While acetylation marks, such as H3K27Ac and H3K14Ac, remained unaffected by manipulations in GAGE12 levels, elevated H3K56Ac levels in f:G12-OE cells were brought back down to levels similar to mock cells when small interfering RNA targeting GAGE (siGAGE) was introduced to reduce GAGE12 levels in these cells (Figure 6B, left panel). These data suggest that GAGE12 expression level alone was able to alter H3K56Ac levels.

Figure 5. Expression of full-length GAGE12 is associated with a more "open" chromatin structure and faster DNA repair dynamics

(A) IR^R and f:G12-OE cells have larger nuclei compared to their P and mock counterparts as indicated by DAPI staining (top panel) and measurement of average nuclei diameter (bottom panel). Scale bar, 10 μm. Nuclei diameters of >100 cells from 3 biological replicates are represented (t test; mean ± SD).

(B) MNase I digestion of chromatin from P versus IR^R (top panel) and mock versus f:G12-OE (bottom panel). Nuclei from 1 × 10^6 cells were isolated and subjected to MNase I digestion at the indicated doses.

(C) Fragment distribution of mock and f:G12-OE cells after ATAC-seq. An enlarged version of the graph focusing on the nucleosome-free regions (NFRs) and Mono nucleosome regions is represented in the right panel.

(D) Pie charts depicting NFR peak distribution in mock versus f:G12-OE cells.

(E) Time-chase resolution of γH2Ax expression post-IR in P versus IR^R (left panel) and mock versus f:G12-OE (right panel). IR^R and f:G12-OE resolved γH2Ax at much faster rates compared to their P and mock counterparts.

(F) Time-chase cell-cycle analysis of P versus IR^R (left panel) and mock versus f:G12-OE (right panel) post-IR. IR^R and f:G12-OE recovers from IR-induced cell cycle arrest at a faster rate compared to their P and mock counterparts (red arrows).

(G) Co-treatment of IR^R and f:G12-OE cells with the ATM inhibitor (ATMi) KU60019 re-sensitized these cells to the cytotoxic effects of IR. Mean ± SD of 3 biological replicates is represented (t test).

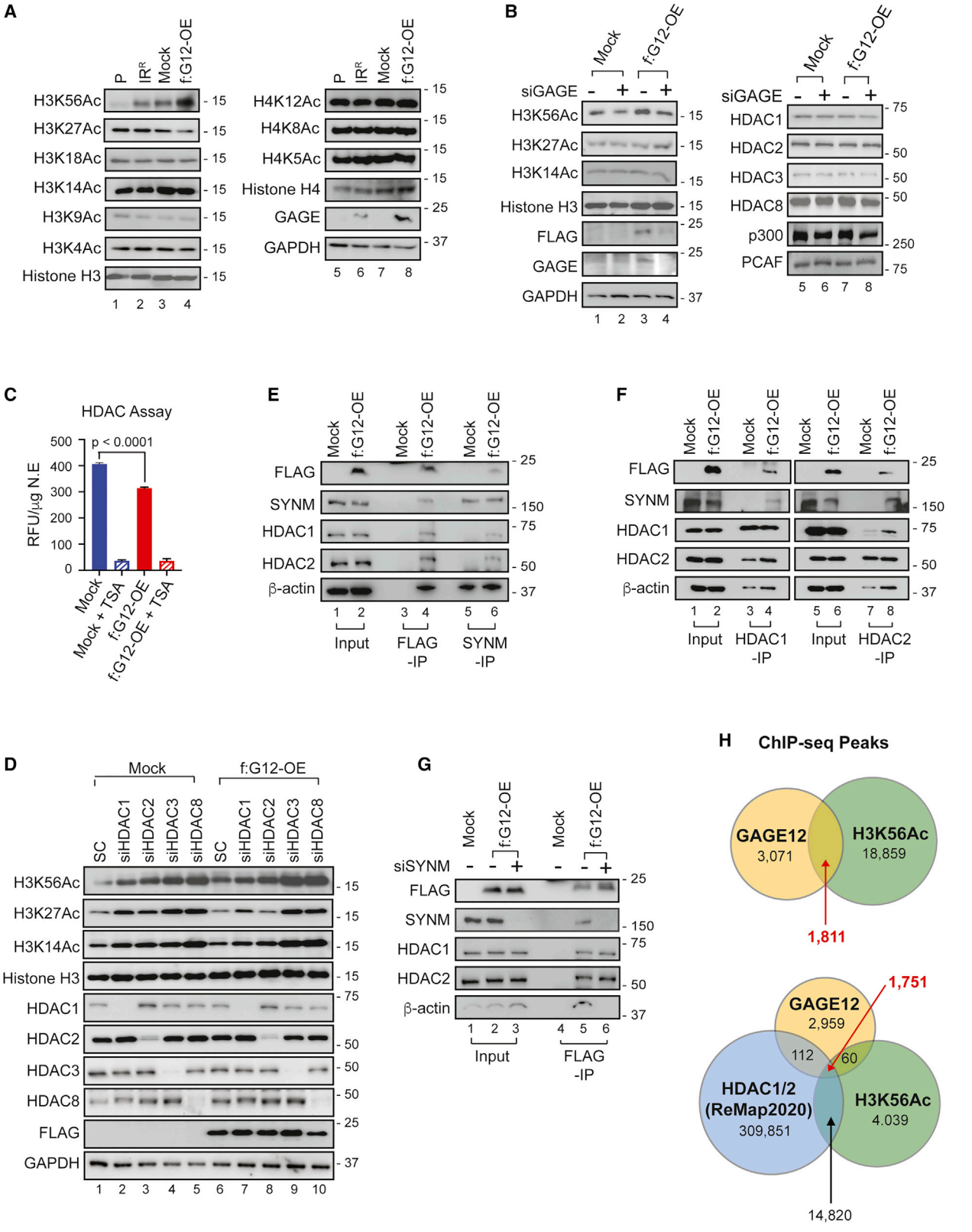

(legend on next page)

Histone acetylation and deacetylation is a dynamic process regulated by histone acetyltransferases (HATs) and HDACs. We next queried whether GAGE12 levels affected the expression of known HDACs and HATs, which may affect H3K56Ac. No significant alterations in the expression of the various class I HDACs (HDAC1, HDAC2, HDAC3, and HDAC8) in mock versus f:G12-OE cells after knockdown of GAGE12 (Figure 6B, right panel, top four rows) were observed. We also did not observe any prominent upregulation in the expressions of p300 and p300-CBP-associated factor (PCAF) (HATs reported to acetylate H3K56; Das et al., 2009). However, we did note a slight decrease in p300 expressions in siGAGE-treated cells (Figure 6B, right panel, bottom two rows). Because expression seemed unaffected, the next assumption would be that the activity of HDACs or HATs may be different in cells that expressed increased levels of GAGE12. Indeed, in *in vitro* enzymatic activity assays to detect HDAC and HAT activity in nuclear lysates of cells overexpressing GAGE12 (f:G12-OE) versus their mock counterparts, there was an observed decrease (~20%) in overall HDAC activity in f:G12-OE cells (Figure 6C). In contrast, overall HAT activity remained the same, regardless of GAGE12 levels (Figure S6B). It was noted that the decrease in HDAC activity was about 20% compared to almost total abrogation of HDAC activity in trichostatin A (TSA) treatment (Figure 6C). This was expected as TSA is a pan class I and II HDAC inhibitor, while in f:G12-OE cells, we only observed deregulation of H3K56Ac. At the same time, other histone acetylation marks remain largely unaffected, suggesting that GAGE12 expression does not inhibit the activity of all HDACs, and this compromised activity may be limited to certain genomic loci.

HDAC1 and HDAC2 are HDACs responsible for the deacetylation of H3K56 (Miller et al., 2010). To better understand which of the HDACs may be involved in the observed elevated H3K56Ac levels in f:G12-OE cells, we performed knockdown of each class I HDAC in mock or f:G12-OE cells. We hypothesized that, if any of the HDACs' activity was compromised at the H3K56Ac sites in f:G12-OE cells, knockdown of the particular HDAC should not increase H3K56Ac levels in f:G12-OE scrambled (SC) versus f:G12-OE HDAC knockdown cells, while an increase in H3K56Ac levels would be observed in mock SC versus mock HDAC knockdown cells. Consistent with our earlier experiments, we first observed elevated H3K56Ac in f:G12-OE SC versus mock SC-treated cells (Figure 6D, lane 1 versus 6), although this phenomenon was not seen at other tested acetylation sites, such as H3K14Ac and H3K27Ac. Next, it was observed that the knockdown of all class I HDACs resulted in an expected notable increase in H3K56Ac in mock cells (Figure 6D, lane 1 versus 2–5). In contrast, although knockdown of HDAC3 and HDAC8 significantly increased H3K56Ac levels in f:G12-OE cells, HDAC1 and HDAC2 knockdown did not considerably upregulate H3K56Ac levels in f:G12-OE cells (Figure 6D, lane 6 versus 7 and 8). These data suggest that the ability of HDAC1/2 to deacetylate H3K56 sites is most likely compromised in f:G12-OE cells, and GAGE12 expression had some inhibitory effects on the ability of HDAC1/2 to deacetylate H3K56, resulting in its constant, elevated levels in f:G12-OE cells. In addition, scrambled knockdown f:G12-OE cells had similar levels of H3K56Ac compared to HDAC1/2 knockdown mock cells (Figure 6D, lane 6 versus 2 and 3), suggesting compromised HDAC1/2 activity at least at some H3K56Ac sites in the f:G12-OE cells. Knockdown of HDAC1 and HDAC2 in f:G12-OE enhanced H3K14Ac and H3K27Ac levels compared to SC-treated f:G12-OE cells, indicating that the most pronounced effects on GAGE12-associated inhibition of HDAC1/2 activity seemed to be at H3K56Ac sites.

To understand how GAGE12 may attenuate HDAC activity, we evaluated the existence of HDAC1 and HDAC2 in the GAGE12-associated complex. In immunoprecipitation experiments using total nuclear extracts from mock and f:G12-OE cells, we observed that both HDAC1 and HDAC2 were present in the complex containing FLAG-GAGE12 and SYNM (Figure 6E). Interestingly, HDAC1 and HDAC2 were only found to be co-immunoprecipitated with SYNM in the presence of GAGE12, as we did not observe the presence of HDAC1 or HDAC2 in SYNM immunoprecipitates obtained from mock cells (Figure 6E, lane 5). To postulate how this interaction between GAGE12, HDAC1/2, and SYNM may inhibit HDAC activity, we considered known interactors of SYNM. HDAC1/2 activity is dependent upon its phosphorylation at specific serine residues. Previously, it was reported that SYNM interacts with PP2A (Pitre et al., 2012), a protein phosphatase known to dephosphorylate HDACs, such as HDAC2 (Yoon et al., 2018). However, we did not find the presence of PP2Ac (the catalytic

Figure 6. GAGE12 modulates H3K56Ac through attenuation of HDAC activity

(A) Expression of various acetyl-histone marks in P versus IR^R and mock versus f:G12-OE cells. Only H3K56 is acetylated at higher levels in IR^R and f:G12-OE cells compared to their P and mock counterparts.

(B) H3K56 acetylation levels are affected by the manipulation of GAGE levels. Overexpression of GAGE12 increased H3K56Ac (lane 1 versus 3) while knockdown of GAGE in f:G12-OE cells return H3K56Ac to levels similar to mock cells (lane 3 versus 4 and 1; left panel). HDAC 1, 2, 3, and 8, as well as HAT and PCAF levels, are not altered by GAGE expression manipulations (right panel).

(C) Total HDAC (left panel) activity in the nuclear extracts of mock versus f:G12-OE cells as measured by *in vitro* HDAC activity assay. Mean ± SD of 3 technical replicates is represented (t test).

(D) H3K56Ac, H3K27Ac, and H3K14Ac levels in mock and f:G12-OE cells after knockdown of each individual class I HDAC.

(E) Interaction of FLAG-GAGE12, SYNM, HDAC1/2, and β-actin in total nuclear lysates of mock and f:G12-OE cells. In FLAG immunoprecipitates, SYNM, HDAC1/2, and β-actin are only pulled down in the presence of FLAG-GAGE12 (lanes 3 and 4). In SYMN immunoprecipitates, SYNM only pulled down HDAC1 and HDAC2 in the presence of FLAG-GAGE12. SYNM interacts with β-actin, even in the absence of GAGE12 (lanes 5 versus 6).

(F) Increased HDAC1-HDAC2-β-actin interaction in the presence of GAGE12. In HDAC1 and HDAC2 immunoprecipitates, increased β-actin was found in the pull-down lysates only in the presence of GAGE12.

(G) Interaction of FLAG-GAGE12, SYNM, HDAC1 and 2, and β-actin in total nuclear lysates of mock and f:G12-OE cells with and without SYNM knockdown. In the absence of SYNM, FLAG-GAGE12 still interacts with HDACs 1 and 2, but not with β-actin (lane 6 versus 5).

(H) Venn diagrams indicating overlapping ChIP-seq peaks in GAGE12 and H3K56Ac ChIPed DNA from f:G12-OE cells (top panel). Venn diagrams indicate co-occupancy of GAGE12 and H3K56Ac with HDAC1/2 in the ReMap2020 datasets (bottom panel).

subunit of PP2A) in the complex containing GAGE12, SYNM, and HDAC1/2 (Figure S6C).

There is now an increasing body of evidence implicating nuclear monomeric actin in regulating chromatin dynamics and transcription via its interactions with RNA polymerase, transcription factors, and chromatin modifiers (de Lanerolle and Serebryannyy, 2011; Kapoor and Shen, 2014). Interestingly, actin was also reported to bind active HDAC1/2 and attenuate its activity, resulting in chromatin unwinding to facilitate gene transcription (Serebryannyy et al., 2016). As SYNM was previously reported to interact with actin (Hijikata et al., 2008), we postulated that actin might be part of the GAGE12, SYNM, HDAC1/2 complex. To this end, we found that actin did exist in the complex containing GAGE12, SYNM, and HDAC1/2 in both HeLa and SiHa cells (Figures 6E, S6C, and S6D). Further, pull-down assays using HDAC1 or HDAC2 as bait revealed that the presence of GAGE12 in f:G12-OE cells seemed to promote HDAC1/2-actin association (Figure 6F, lanes 4 and 8). Intriguingly, we observed actin interaction with SYNM in the absence of GAGE12 (Figure 6E, lane 5), while in the absence of SYNM, GAGE12 interacted with HDAC1/2, but not actin (Figure 6G). To validate that GAGE12 and H3K56Ac do co-occupy certain sites on the chromatin, chromatin immunoprecipitation followed by sequencing (ChIP-seq) was performed using anti-FLAG and anti-H3K56Ac antibodies in f:G12-OE HeLa cells. The FLAG-tagged GAGE12 was used as bait here for ChIP studies due to the unavailability of ChIP-grade endogenous GAGE antibodies. Here, it was observed that approximately 35% of ChIPed chromatin-bound GAGE12 overlapped with H3K56Ac sites (Figure 6H, top panel). This was consistent with the approximate 30% increase in transposase accessible peaks in our ATAC-seq experiments (Figure 5C). Moreover, reanalysis of our f:GAGE12 and H3K56Ac ChIP-seq data with available ChIP-seq data for HDAC1/2 in the ReMap2020 database (Chèneby et al., 2020) further showed that GAGE12, H3K56Ac, and HDAC1/2 did indeed co-occupy certain sites on the chromatin. More importantly, >95% of GAGE12-H3K56Ac co-occupancy peaks also co-occupy HDAC1/2 sites (Figure 6H, bottom panel). Taken together, our protein interaction and ChIP-seq studies suggest that GAGE12 may act as an intermediary in a complex that associates HDAC1/2 with actin, thus inhibiting HADC1/2's ability to bring about H3K56 deacetylation at specific genetic loci where the components of this complex co-occupy.

We have earlier shown that the dissolution of GAGE12-SYNM-HDAC1/2-actin complex via the loss of SYNM expression (Figure 6G) resulted in the re-sensitization of f:G12-OE cells to the cytotoxic effects of IR (Figure 4G). Jasplakinolide is a cyclodepsipeptide isolated from *Jaspis johnstoni*, previously reported to promote actin hyper-polymerization and cytotoxicity in combination with IR in prostate and Lewis lung cancer cells (Senderowicz et al., 1995; Stehn et al., 2013; Takeuchi et al., 1998). Therefore, we hypothesized that jasplakinolide could disrupt the complex formation by reducing the nuclear monomeric actin pool, preventing its interaction with HDAC1/2 in the GAGE12-SYNM-HDAC1/2-actin complex. Indeed, the combination of jasplakinolide treatment at IC20 (20% maximal inhibitory concentration) dose (Figure S6E) with IR re-sensitized f:G12-OE cells to IR (Figure 7A). We noted that, although there is a reduction of actin levels in the nucleus of f:G12-OE cells after jasplakinolide treatment (NP and Chro fractions in Figure 7B, lanes 7 and 8 versus lanes 3 and 4), we also noticed the loss of SYNM and f:GAGE12 in the same fractions with jasplakinolide treatment (Figure 7B). This could be due to SYNM's interaction with actin. Despite this, jasplakinolide treatment further demonstrated that the loss of GAGE12 in the chromatin does indeed result in the re-sensitization of f:G12-OE cells to IR, highlighting the essential role of this GAGE12-associated complex in conferring the IR-resistance phenotype in CC.

DISCUSSION

Figure 7C summarizes the mechanistic findings of this study. In GAGE12-high cells (Figure 7C, left panel), GAGE12 acts as an intermediary between HDAC1/2 and its inhibitor actin at certain H3K56Ac sites, resulting in compromised HDAC1/2 function and sustained elevated levels of H3K56Ac at these sites. This elevated H3K56Ac results in a more open chromatin structure and increased DNA damage repair efficiency. This increases the cell's tolerance to IR-induced DNA damage cumulating to the IR-resistant phenotype. In contrast, in GAGE12-low cells (Figure 7C, right panel), there is a homeostatic balance between H3K56 acetylation and deacetylation by HATs and HDACs, maintaining a more compact chromatin structure. Upon IR insult, the DNA damage response is activated, and cell death is induced when cells cannot repair the damage.

Mechanistically, this study provides insights into the molecular functions of the GAGE family of proteins, including functional differences between protein variants encoded by this highly homologous family of transcripts. We showed that specific chromatin localization of the GAGE12 protein variant is important in conferring the IR-resistant phenotype. Through mass spectrometry analysis, we identified intermediate filament (IF) SYNM as the molecule involved in localizing GAGE12 to the chromatin. Though IFs are typically located in the cytoplasm and nuclear envelope, SYNM has been reported to exhibit nuclear localization in glioblastomas (Pitre et al., 2012) and head and neck cancer cells (Deville et al., 2020). Although how SYNM is localized to the nucleus remains to be elucidated, IFs, such as desmin, that interact with SYNM have also been reported to localize to the nucleus with observed gene regulatory functions (Li et al., 1994). Therefore, it is a reasonable assumption that, in IR-resistant CC cells, SYNM and GAGE12 interaction localizes the GAGE12-SYNM complex to specific DNA loci to elicit alterations in chromatin structure by bringing HDAC1/2 into close proximity with its inhibitor actin. With the recent discovery that SYNM affects non-homologous end joining (NHEJ) in head and neck cancer cells (Deville et al., 2020), it will be interesting to study whether GAGE12 is also involved in the NHEJ pathway, which may contribute to IR resistance.

Here, we also demonstrate the role of GAGE12 in altering chromatin structure, thereby increasing the efficiency of DNA damage repair, resulting in resistance to IR-induced cell death (Figure 5). H3K56Ac level was shown to be elevated in GAGE12-overexpressing cells (Figures 6A and S6A) and is directly affected by manipulations of GAGE12 levels (Figure 6B). H3K56Ac is a histone mark associated with DNA damage

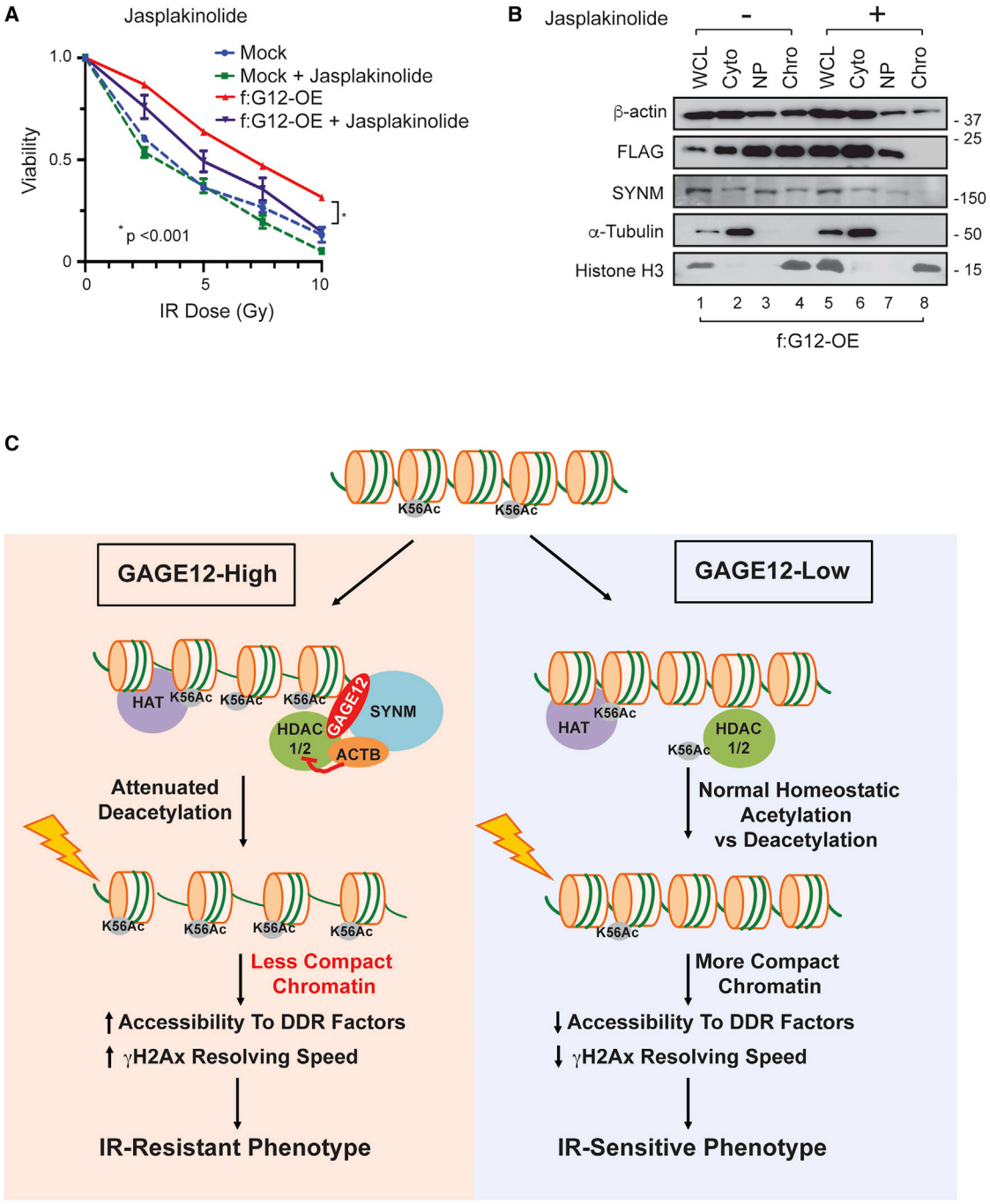

Figure 7. Pharmacological inhibition of the GAGE12-SYNM-HDAC1/2-actin complex re-sensitizes cells to IR

(A) Re-sensitization of f:G12-OE cells to IR after jasplakinolide treatment. Viability is measured 3 days post-IR. IC20 dose for jasplakinolide was used. Mean ± SD of 3 biological replicates is represented (t test).

(B) Loss of chromatin localization of f:GAGE12 in f:G12-OE cells after jasplakinolide treatment analyzed after fractionation.

(C) Proposed mode of action for GAGE12-mediated IR resistance in cervical cancer cells.

response (Vempati et al., 2010; Wurtele et al., 2012) and chromatin disassembly (Williams et al., 2008). Although the exact role of H3K56Ac in DNA repair in response to different DNA damage reagents remains controversial, there is at least some consensus that H3K56Ac is a mark of less condensed chromatin. Our data suggest that GAGE12 could be an intermediary molecule that brings HDAC1/2 to its inhibitor actin. GAGE12-SYNM-HDAC1/2-actin interaction sustains H3K56Ac

in GAGE12-expressing cells, resulting in a more decondensed chromatin structure, increased DNA machinery accessibility, and improved DNA repair efficiency. A recent study identified Tripartite-motif-containing 66 (TRIM66), a member of the tripartite motif family of proteins, as a reader of H3K56Ac in embryonic stem cells (ESCs). Here, TRIM66 promotes the deacetylation of H3K56Ac by Sirtuin 6 (SIRT6) after DNA damage and promotes repair in ESCs (Chen et al., 2019). Similar to ESCs, f:G12-OE cells had endogenously elevated levels of H3K56Ac. Intriguingly, we too noticed rapid deacetylation of H3K56Ac in these cells post-IR coupled with earlier pATM induction and resolution (Figure S5F), suggesting that the TRIM66-mediated DNA damage response may contribute to increased repair efficiency in these cells. H3K56Ac is also a mark for active transcription and revealed to have functions in regulating ESC pluripotency (Jain et al., 2016; Tan et al., 2013; Xie et al., 2009). Our observations that GAGE12 regulates H3K56Ac and co-occupies certain gene loci (Figure 6) could imply that GAGE12 may have gene-regulatory functions. Previous studies suggest that knockdown of GAGE12 in gastric cancer cells (Lee et al., 2015) affected the expression of genes involved in epithelial to mesenchymal transition, highlighting the potential role of GAGE12 in gene regulation. Emerging data from our laboratory combining ATAC, ChIP, and RNA-seq suggest that GAGE12-mediated H3K56Ac may have potential roles in regulating some of these genes. However, more needs to be done to better understand the role of GAGE12 in the regulation of H3K56Ac and transcription. In terms of its role in regulating chromatin dynamics, interrogation of the ReMap2020 datasets with our GAGE12 ChIP-seq data suggests that GAGE12 also showed co-occupancy with several chromatin modifiers and lysine demethylases. This indicates that CT antigens, such as GAGE, may have more widespread functions in regulating chromatin structure.

This study also demonstrated that disruption of GAGE12 localization and thus loss of HDAC1/2-actin interaction via SYNM knockdown re-sensitized f:G12-OE cells to IR (Figures 4G, 6G, and S4C). Treatment of f:G12-OE with jasplakinolide, which promotes actin polymerization and decreases levels of monomeric nuclear actin available for HDAC inhibition, also re-sensitized f:G12-OE to IR (Figures 7A and 7B). However, we were unable to attribute the re-sensitization effects of jasplakinolide solely to the inhibition of HDAC1/2 by actin as jasplakinolide also decreased SYNM nuclear expression and hence also reduced GAGE12 levels in the nucleus (Figure 7B). However, this observation suggests that pharmacologic agents that disrupt the formation of the GAGE12-SYNM-HDAC1/2-actin complex could potentially be developed as radiosensitizers for therapeutic intervention.

Clinically, despite RT's success in curtailing progression in CC, treatment failure attributed to RT resistance still occurs in a considerable proportion of patients. Molecular alterations have been implicated in the adaptation of cellular response to RT. In this study, unbiased genetic screening of IR-sensitive versus resistant xenograft tumors identified GAGE as a possible early predictor of distant treatment failure in CC. Although IR-resistant cell line models were generated by repeated irradiation, the observed elevated levels of GAGE expression in RT-resistant pre-treatment clinical samples (Figures 1H, 1I, and S3E) suggests that higher GAGE expression could predict *de novo* RT resistance. This was further validated in cell lines where overexpression of GAGE12 alone was able to confer the IR-resistant phenotype (Figures 2 and S3A). Potentially, GAGE may be clinically translated as a predictive biomarker for RT response to predict treatment outcomes from standard RT pre-treatment. Identifying patients with high GAGE expression and who may be poor responders to standard RT at diagnosis could improve treatment outcomes by providing clinicians with the opportunity to tailor treatment options and escalate required RT doses in a timelier manner.

In summary, our data showed that GAGE12 mediates the radio-resistant phenotype in the cervical cancer model. This effect was attributed to GAGE12's role in inhibiting HDAC1/2 function, consequently increasing chromatin decompaction and DNA-repair efficiency. Clinically, we found that elevated GAGE levels positively correlated with local and/or distant treatment failure in pre-treatment biopsy samples, suggesting its potential application as a predictive marker for radiotherapy response in cervical cancer. Lastly, our mechanistic studies highlighted potential therapeutic opportunities to utilize agents that target GAGE or the GAGE-associated complex in combination with RT to improve outcomes.

STAR★METHODS

Detailed methods are provided in the online version of this paper and include the following:

- KEY RESOURCES TABLE
- RESOURCE AVAILABILITY
  - Lead contact
  - Materials availability
  - Data and code availability
- EXPERIMENTAL MODEL AND SUBJECT DETAILS
  - Cell culture and generation IR-resistant cell lines
  - Mice
- METHOD DETAILS
  - Constructs, infection and transfection of human cell lines
  - Xenograft models and microarray analysis
  - qRT-PCR
  - Clinical samples, RNA analysis and immunohistochemistry
  - 2D viability and long-term colony formation assays
  - 3D anchorage-independent and tumorsphere formation assays
  - Generation of the pan-GAGE monoclonal antibody (GA-1a)
  - Western blot analysis
  - Immunofluorescence staining
  - Cellular fractionation
  - Mass spectrometry
  - Immunoprecipitation
  - Micrococcal Nuclease I (MNaseI) Digestion Assay
  - Assay of Transposase Accessible Chromatin (ATAC) and Chromatin Immunoprecipitation (ChIP) sequencing

- Cell cycle analysis
- *In vitro* HDAC and HAT Assay
- siRNAs and gene knockdown
- ATM inhibitor (KU60019) and Jasplakinolide treatment

● QUANTIFICATION AND STATISTICAL ANALYSIS

SUPPLEMENTAL INFORMATION

Supplemental information can be found online at https://doi.org/10.1016/j.celrep.2021.109621.

ACKNOWLEDGMENTS

This work was supported by grants from the Terry Fox Foundation Singapore (NF15TFR051) to B.A.C., National University Hospital, Singapore, Junior Pitch for Fund to C.W., National University Health System, Singapore (R-183-000-461-733) to D.S.N., and the Ministry of Education, Singapore; (MOE-AcRF-Tier 2 and R-183-000-459-112) and National University Cancer Institute, Singapore (NR15NMR229 and NR18NMR119) to L.-W.D.

AUTHOR CONTRIBUTIONS

Conceptualization, D.S.N., C.W., B.A.C., and L.-W.D.; performed experiments, D.S.N., S.B.I., Z.-W.L., Z.M.D., J.M.A.D., and W.W.; IHC analysis, D.L.; clinical sample collection and analysis, C.W., J.S.-Y.N., J.J.H.L., Y.H.L., D.S.P.T., and B.A.C.; GAGE antibody generation and validation, K.-Y.W. and S.-C.C.; reagents and discussion, D.S.P.T. and S.J.; data analysis, D.S.N., C.W., T.Z.T., W.W., and J.M.A.D.; writing, D.S.N. and L.-W.D.; reviewing, all authors; supervision, L.-W.D.

DECLARATION OF INTERESTS

The authors declare no competing interests.

Received: September 8, 2020
Revised: June 3, 2021
Accepted: August 5, 2021
Published: August 31, 2021

REFERENCES

Banerjee, R., and Kamrava, M. (2014). Brachytherapy in the treatment of cervical cancer: a review. Int. J. Womens Health *6*, 555–564.

Baskar, R., Lee, K.A., Yeo, R., and Yeoh, K.-W. (2012). Cancer and radiation therapy: current advances and future directions. Int. J. Med. Sci. *9*, 193–199.

Boël, P., Wildmann, C., Sensi, M.L., Brasseur, R., Renauld, J.-C., Coulie, P., Boon, T., and van der Bruggen, P. (1995). BAGE: a new gene encoding an antigen recognized on human melanomas by cytolytic T lymphocytes. Immunity *2*, 167–175.

Chen, Y.-T., Scanlan, M.J., Venditti, C.A., Chua, R., Theiler, G., Stevenson, B.J., Iseli, C., Gure, A.O., Vasicek, T., Strausberg, R.L., et al. (2005). Identification of cancer/testis-antigen genes by massively parallel signature sequencing. Proc. Natl. Acad. Sci. USA *102*, 7940–7945.

Chen, J., Wang, Z., Guo, X., Li, F., Wei, Q., Chen, X., Gong, D., Xu, Y., Chen, W., Liu, Y., et al. (2019). TRIM66 reads unmodified H3R2K4 and H3K56ac to respond to DNA damage in embryonic stem cells. Nat. Commun. *10*, 4273.

Chèneby, J., Ménétrier, Z., Mestdagh, M., Rosnet, T., Douida, A., Rhalloussi, W., Bergon, A., Lopez, F., and Ballester, B. (2020). ReMap 2020: a database of regulatory regions from an integrative analysis of Human and Arabidopsis DNA-binding sequencing experiments. Nucleic Acids Res. *48* (*D1*), D180–D188.

Chiang, Y.-W., Li, C.-J., Su, H.-Y., Hsieh, K.-T., Weng, C.-W., Chen, H.-W., and Chang, S.-C. (2021). Development of mouse monoclonal antibody for detecting hemagglutinin of avian influenza A(H7N9) virus and preventing virus infection. Appl. Microbiol. Biotechnol. *105*, 3235–3248.

Chiu, Y.H., Lee, J.Y., and Cantley, L.C. (2014). BRD7, a tumor suppressor, interacts with p85α and regulates PI3K activity. Mol. Cell *54*, 193–202.

Cho, O., and Chun, M. (2018). Management for locally advanced cervical cancer: new trends and controversial issues. Radiat. Oncol. J. *36*, 254–264.

Cilensek, Z.M., Yehiely, F., Kular, R.K., and Deiss, L.P. (2002). A member of the GAGE family of tumor antigens is an anti-apoptotic gene that confers resistance to Fas/CD95/APO-1, Interferon-gamma, taxol and gamma-irradiation. Cancer Biol. Ther. *1*, 380–387.

Coulie, P.G., Weynants, P., Lehmann, F., Herman, J., Brichard, V., Wölfel, T., Van Pel, A., De Plaen, E., Brasseur, F., and Boon, T. (1993). Genes coding for tumor antigens recognized by human cytolytic T lymphocytes. J. Immunother. Emphasis Tumor Immunol. *14*, 104–109.

da Silva, V.L., Fonseca, A.F., Fonseca, M., da Silva, T.E., Coelho, A.C., Kroll, J.E., de Souza, J.E.S., Stransky, B., de Souza, G.A., and de Souza, S.J. (2017). Genome-wide identification of cancer/testis genes and their association with prognosis in a pan-cancer analysis. Oncotarget *8*, 92966–92977.

Das, C., Lucia, M.S., Hansen, K.C., and Tyler, J.K. (2009). CBP/p300-mediated acetylation of histone H3 on lysine 56. Nature *459*, 113–117.

De Backer, O., Arden, K.C., Boretti, M., Vantomme, V., De Smet, C., Czekay, S., Viars, C.S., De Plaen, E., Brasseur, F., Chomez, P., et al. (1999). Characterization of the GAGE genes that are expressed in various human cancers and in normal testis. Cancer Res. *59*, 3157–3165.

de Lanerolle, P., and Serebryannyy, L. (2011). Nuclear actin and myosins: life without filaments. Nat. Cell Biol. *13*, 1282–1288.

Deville, S.S., Vehlow, A., Förster, S., Dickreuter, E., Borgmann, K., and Cordes, N. (2020). The intermediate filament synemin regulates non-homologous end joining in an ATM-dependent manner. Cancers (Basel) *12*, 1717.

Eichmüller, S., Usener, D., Jochim, A., and Schadendorf, D. (2002). mRNA expression of tumor-associated antigens in melanoma tissues and cell lines. Exp. Dermatol. *11*, 292–301.

Floyd, S.R., Pacold, M.E., Huang, Q., Clarke, S.M., Lam, F.C., Cannell, I.G., Bryson, B.D., Rameseder, J., Lee, M.J., Blake, E.J., et al. (2013). The bromodomain protein Brd4 insulates chromatin from DNA damage signalling. Nature *498*, 246–250.

Gjerstorff, M.F., and Ditzel, H.J. (2008). An overview of the GAGE cancer/testis antigen family with the inclusion of newly identified members. Tissue Antigens *71*, 187–192.

Hijikata, T., Nakamura, A., Isokawa, K., Imamura, M., Yuasa, K., Ishikawa, R., Kohama, K., Takeda, S., and Yorifuji, H. (2008). Plectin 1 links intermediate filaments to costameric sarcolemma through beta-synemin, alpha-dystrobrevin and actin. J. Cell Sci. *121*, 2062–2074.

Hofmann, O., Caballero, O.L., Stevenson, B.J., Chen, Y.-T., Cohen, T., Chua, R., Maher, C.A., Panji, S., Schaefer, U., Kruger, A., et al. (2008). Genome-wide analysis of cancer/testis gene expression. Proc. Natl. Acad. Sci. USA *105*, 20422–20427.

Jain, A.K., Xi, Y., McCarthy, R., Allton, K., Akdemir, K.C., Patel, L.R., Aronow, B., Lin, C., Li, W., Yang, L., and Barton, M.C. (2016). LncPRESS1 is a p53-regulated lncRNA that safeguards pluripotency by disrupting SIRT6-mediated de-acetylation of histone H3K56. Mol. Cell *64*, 967–981.

Kapoor, P., and Shen, X. (2014). Mechanisms of nuclear actin in chromatin-remodeling complexes. Trends Cell Biol. *24*, 238–246.

Kubo, K., Koiwai, S., and Morita, K. (1982). Mechanism of derivation of radioresistance in HeLa cell population after repeated x-irradiation. J. Radiat. Res. (Tokyo) *23*, 204–217.

Landt, S.G., Marinov, G.K., Kundaje, A., Kheradpour, P., Pauli, F., Batzoglou, S., Bernstein, B.E., Bickel, P., Brown, J.B., Cayting, P., et al. (2012). ChIP-seq guidelines and practices of the ENCODE and modENCODE consortia. Genome Res. *22*, 1813–1831.

Lea, J.S., and Lin, K.Y. (2012). Cervical cancer. Obstet. Gynecol. Clin. North Am. *39*, 233–253.

Lee, E.K., Song, K.A., Chae, J.H., Kim, K.M., Kim, S.H., and Kang, M.S. (2015). GAGE12 mediates human gastric carcinoma growth and metastasis. Int. J. Cancer *136*, 2284–2292.

Li, H., and Durbin, R. (2009). Fast and accurate short read alignment with Burrows-Wheeler transform. Bioinformatics *25*, 1754–1760.

Li, H., Choudhary, S.K., Milner, D.J., Munir, M.I., Kuisk, I.R., and Capetanaki, Y. (1994). Inhibition of desmin expression blocks myoblast fusion and interferes with the myogenic regulators MyoD and myogenin. J. Cell Biol. *124*, 827–841.

Liu, M., Hu, Z., Qi, L., Wang, J., Zhou, T., Guo, Y., Zeng, Y., Zheng, B., Wu, Y., Zhang, P., et al. (2013). Scanning of novel cancer/testis proteins by human testis proteomic analysis. Proteomics *13*, 1200–1210.

Miller, K.M., Tjeertes, J.V., Coates, J., Legube, G., Polo, S.E., Britton, S., and Jackson, S.P. (2010). Human HDAC1 and HDAC2 function in the DNA-damage response to promote DNA nonhomologous end-joining. Nat. Struct. Mol. Biol. *17*, 1144–1151.

Moreno-Acosta, P., Gamboa, O., Sanchez de Gomez, M., Cendales, R., Diaz, G.D., Romero, A., Balart Serra, J., Conrado, Z., Levy, A., Chargari, C., and Magné, N. (2012). IGF1R gene expression as a predictive marker of response to ionizing radiation for patients with locally advanced HPV16-positive cervical cancer. Anticancer Res. *32*, 4319–4325.

Nicolay, N.H., Carter, R., Hatch, S.B., Schultz, N., Prevo, R., McKenna, W.G., Helleday, T., and Sharma, R.A. (2012). Homologous recombination mediates S-phase-dependent radioresistance in cells deficient in DNA polymerase eta. Carcinogenesis *33*, 2026–2034.

Pitre, A., Davis, N., Paul, M., Orr, A.W., and Skalli, O. (2012). Synemin promotes AKT-dependent glioblastoma cell proliferation by antagonizing PP2A. Mol. Biol. Cell *23*, 1243–1253.

Quinlan, A.R., and Hall, I.M. (2010). BEDTools: a flexible suite of utilities for comparing genomic features. Bioinformatics *26*, 841–842.

Rogers, P.B., Plowman, P.N., Harris, S.J., and Arlett, C.F. (2000). Four radiation hypersensitivity cases and their implications for clinical radiotherapy. Radiother. Oncol. *57*, 143–154.

Scanlan, M.J.G., Simpson, A.J., and Old, L.J. (2004). The cancer/testis genes: review, standardization, and commentary. Cancer Immun. *4*, 1.

Senderowicz, A.M.J., Kaur, G., Sainz, E., Laing, C., Inman, W.D., Rodríguez, J., Crews, P., Malspeis, L., Grever, M.R., Sausville, E.A., et al. (1995). Jasplakinolide's inhibition of the growth of prostate carcinoma cells in vitro with disruption of the actin cytoskeleton. J. Natl. Cancer Inst. *87*, 46–51.

Serebryannyy, L.A., Cruz, C.M., and de Lanerolle, P. (2016). A role for nuclear actin in HDAC 1 and 2 regulation. Sci. Rep. *6*, 28460.

Shi, D.B., Ma, R.R., Zhang, H., Hou, F., Guo, X.Y., and Gao, P. (2019). GAGE7B promotes tumor metastasis and growth via activating the p38δ/pMAPKAPK2/pHSP27 pathway in gastric cancer. J. Exp. Clin. Cancer Res. *38*, 124–136.

Simpson, A.J.G., Caballero, O.L., Jungbluth, A., Chen, Y.-T., and Old, L.J. (2005). Cancer/testis antigens, gametogenesis and cancer. Nat. Rev. Cancer *5*, 615–625.

Stehn, J.R., Haass, N.K., Bonello, T., Desouza, M., Kottyan, G., Treutlein, H., Zeng, J., Nascimento, P.R.B.B., Sequeira, V.B., Butler, T.L., et al. (2013). A novel class of anticancer compounds targets the actin cytoskeleton in tumor cells. Cancer Res. *73*, 5169–5182.

Taguchi, A., Taylor, A.D., Rodriguez, J., Celiktaş, M., Liu, H., Ma, X., Zhang, Q., Wong, C.-H., Chin, A., Girard, L., et al. (2014). A search for novel cancer/testis antigens in lung cancer identifies VCX/Y genes, expanding the repertoire of potential immunotherapeutic targets. Cancer Res. *74*, 4694–4705.

Takeuchi, H., Ara, G., Sausville, E.A., and Teicher, B. (1998). Jasplakinolide: interaction with radiation and hyperthermia in human prostate carcinoma and Lewis lung carcinoma. Cancer Chemother. Pharmacol. *42*, 491–496.

Tan, Y., Xue, Y., Song, C., and Grunstein, M. (2013). Acetylated histone H3K56 interacts with Oct4 to promote mouse embryonic stem cell pluripotency. Proc. Natl. Acad. Sci. USA *110*, 11493–11498.

Vempati, R.K., Jayani, R.S., Notani, D., Sengupta, A., Galande, S., and Haldar, D. (2010). p300-mediated acetylation of histone H3 lysine 56 functions in DNA damage response in mammals. J. Biol. Chem. *285*, 28553–28564.

Wang, R., Li, Q., Helfer, C.M., Jiao, J., and You, J. (2012). Bromodomain protein Brd4 associated with acetylated chromatin is important for maintenance of higher-order chromatin structure. J. Biol. Chem. *287*, 10738–10752.

West, C.M., Elyan, S.A., Berry, P., Cowan, R., and Scott, D. (1995). A comparison of the radiosensitivity of lymphocytes from normal donors, cancer patients, individuals with ataxia-telangiectasia (A-T) and A-T heterozygotes. Int. J. Radiat. Biol. *68*, 197–203.

Williams, S.K., Truong, D., and Tyler, J.K. (2008). Acetylation in the globular core of histone H3 on lysine-56 promotes chromatin disassembly during transcriptional activation. Proc. Natl. Acad. Sci. USA *105*, 9000–9005.

Williamson, E.A., Wray, J.W., Bansal, P., and Hromas, R. (2012). Overview for the histone codes for DNA repair. Prog. Mol. Biol. Transl. Sci. *110*, 207–227.

Wurtele, H., Kaiser, G.S., Bacal, J., St-Hilaire, E., Lee, E.H., Tsao, S., Dorn, J., Maddox, P., Lisby, M., Pasero, P., and Verreault, A. (2012). Histone H3 lysine 56 acetylation and the response to DNA replication fork damage. Mol. Cell. Biol. *32*, 154–172.

Xie, W., Song, C., Young, N.L., Sperling, A.S., Xu, F., Sridharan, R., Conway, A.E., Garcia, B.A., Plath, K., Clark, A.T., et al. (2009). Histone h3 lysine 56 acetylation is linked to the core transcriptional network in human embryonic stem cells. Mol. Cell *33*, 417–427.

Yoon, S., Kook, T., Min, H.K., Kwon, D.H., Cho, Y.K., Kim, M., Shin, S., Joung, H., Jeong, S.H., Lee, S., et al. (2018). PP2A negatively regulates the hypertrophic response by dephosphorylating HDAC2 S394 in the heart. Exp. Mol. Med. *50*, 1–14.

Zhang, Y., Liu, T., Meyer, C.A., Eeckhoute, J., Johnson, D.S., Bernstein, B.E., Nusbaum, C., Myers, R.M., Brown, M., Li, W., and Liu, X.S. (2008). Model-based analysis of ChIP-Seq (MACS). Genome Biol. *9*, R137.

STAR★METHODS

KEY RESOURCES TABLE

REAGENT or RESOURCE	SOURCE	IDENTIFIER
Antibodies		
Rabbit polyclonal α-GAGE12B	Thermo Fisher Scientific	Cat# PA5-48149; RRID: AB_2633607
Rabbit polyclonal α-GAGE12H	Thermo Fisher Scientific	Cat# PA5-48611; RRID: AB_2634068
Rabbit polyclonal α-GAPDH (clone FL-335)	Santa Cruz Biotechnology	Cat. #sc-25778; RRID: AB_10167668
Mouse polyclonal α-FLAG	Sigma-Aldrich	Cat. #F3165; RRID: AB_259529
Mouse monoclonal α- alpha Tubulin (B-7) antibody	Santa Cruz Biotechnology	Cat. # sc-5286; RRID: AB_628411
Rabbit monoclonal α-Histone H3	Cell Signaling Technology	Cat. #4499; RRID: AB_10544537
Mouse monoclonal α-Desmuslin (A8)/SYNM	Santa Cruz Biotechnology	Cat. #sc- 374484; RRID: AB_10989943
Rabbit monoclonal α-Phospho-Histone H2A.X (Ser139)	Cell Signaling Technology	Cat. Cat. #9718; RRID: AB_10121789.
Rabbit polyclonal α- Acetyl-Histone H3 (Lys56) Antibody	Cell Signaling Technology	Cat# 4243; RRID: AB_10548193
Rabbit polyclonal α- Acetyl-Histone H3 (Lys27) Antibody	Cell Signaling Technology	Cat# 4353; RRID: AB_10545273
Rabbit polyclonal α- Acetyl-Histone H3 (Lys18) (D8Z5H) antibody	Cell Signaling Technology	Cat# 13998; RRID: AB_2783723
Rabbit monoclonal α-Acetyl-Histone H3 (Lys14) (D4B9)	Cell Signaling Technology	Cat# 7627; RRID: AB_10839410
Rabbit monoclonal Acetyl-Histone H3 (Lys9) (C5B11)	Cell Signaling Technology	Cat. #9649; RRID: AB_823528
Rabbit polyclonal α- Acetyl-Histone H3 (Lys4)	Active Motif	Cat. #39381; RRID: AB_2793236
Rabbit polyclonal α- Acetyl-Histone H4 (Lys12)	Cell Signaling Technology	Cat# 2591; RRID: AB_2118617
Rabbit polyclonal α- Acetyl-Histone H4 (Lys8)	Cell Signaling Technology	Cat# 2594; RRID: AB_2248400
Rabbit polyclonal α- Acetyl-Histone H4 (Lys5)	Cell Signaling Technology	Cat# 9672; RRID: AB_10622616
Mouse monoclonal α- Anti-Histone H4	Cell Signaling Technology	Cat# 2935; RRID: AB_1147658
Mouse monoclonal α- HDAC1 (10E2)	Cell Signaling Technology	Cat# 5356; RRID: AB_10612242
Mouse monoclonal α- HDAC2 (3F3)	Cell Signaling Technology	Cat# 5113; RRID: AB_1062487
Mouse monoclonal α- HDAC3 (7G6C5)	Cell Signaling Technology	Cat# 3949; RRID: AB_2118371
Rabbit polyclonal α- HDAC8	Millipore	Cat# 07-505; RRID: AB_11213347
Mouse monoclonal α- Anti-p300 CT, clone RW128	Millipore	Cat# 05-257; RRID: AB_11213111
Rabbit monoclonal α- Acetyl-PCAF (C14G9)	Cell Signaling Technology	Cat# 3378; RRID: AB_2128409
Mouse monoclonal α- beta-Actin, Clone AC-74	Sigma-Aldrich	Cat# A5316; RRID: AB_47674
Rabbit polyclonal α-GAGE12B (N-term)	Abgent	Cat# AP11254a; RRID: AB_10821403
Mouse monoclonal α- PP2A, C subunit, clone 1D6	Millipore	Cat# 05-421; RRID: AB_309726
Rabbit monoclonal α- Phospho-ATM (Ser1981) (D25E5)	Cell Signaling Technology	Cat# 13050, RRID:AB_2798100
Rabbit monoclonal α- Phospho-Chk2 (Thr68) (C13C1)	Cell Signaling Technology	Cat# 2197, RRID:AB_2080501
Rabbit polyclonal α- Acetyl-Histone H3 (Lys56) Antibody	Active Motif	Cat# 39281, RRID:AB_2661786
Mouse monoclonal α-pan-GAGE antibody (Clone GA-1a)	Laboratory of Dr. Shih-Chung Chang, National Taiwan University	This paper
Chemicals, peptides, and recombinant proteins		
Trichostatin A	Sigma-Aldrich	Cat. # T8552; CAS 58880-19-6
Jasplakinolide	Merck Millipore	Cat. #420107; CAS 102396-24-7
KU-60019	Sigma-Aldrich	Cat. # SML1416; CAS 925701-49-1

(*Continued on next page*)

Continued

REAGENT or RESOURCE	SOURCE	IDENTIFIER
Critical commercial assays		
In vitro HDAC Activity Assay Kit	Biovision	Cat. #K330-100
In vitro HAT Activity Assay Kit	Biovision	#K334-100
Expression profiling microarray	Illumina	Illumina HT12v4
Deposited data		
Raw and unprocessed data including microarray datasets, Mass-spectrometry identifications and western blot data.	Mendeley Data	https://doi.org/10.17632/jxnnzrzwzf.3
Microarray dataset	GEO	GEO: GSE181080
Experimental models: Cell lines		
HeLa	ATCC	ATCC® CCL-2
SiHa	ATCC	ATCC # HTB-35
Experimental models: Organisms/strains		
BALB/c female nude mice	*In Vivo*s Pte Ltd	N/A
Oligonucleotides		
Please see Table S1 for oligonucleotide information		N/A
Recombinant DNA		
pLenti CMV GFP Puro (658-5)	Laboratory of Dr. Su, I-Hsin, Nanyang Technological University, Singapore	Addgene_17448
pMD.G	Laboratory of Dr. Su, I-Hsin, Nanyang Technological University, Singapore	N/A
dR8.91	Laboratory of Dr. Su, I-Hsin, Nanyang Technological University, Singapore	N/A
Software and algorithms		
GraphPad Prism 8.0	GraphPad Software	https://www.graphpad.com
bwa v0.7.13-r1126 aligner	Li and Durbin, 2009	http://maq.sourceforge.net
Picard v2.28.0	This paper	http://broadinstitute.github.io/picard/
MACS2 v2.1.4	Zhang et al., 2008	https://github.com/macs3-project/MACS
phantompeakqualtools v1.0	Landt et al., 2012	N/A
BEDTools suite	Quinlan and Hall, 2010	https://code.google.com/archive/p/bedtools

RESOURCE AVAILABILITY

Lead contact

Further information and requests for resources and reagents should be directed to and will be fulfilled by Lead Contact Lih-Wen Deng (bchdlw@nus.edu.sg).

Materials availability

All plasmids and cell lines generated in this study will be made available on request to the Lead author with a completed Materials Transfer Agreement. A completed Materials Transfer Agreement or Research Collaboration Agreement with the National University of Singapore and the National Taiwan University will be required for sharing of the mouse monoclonal pan-GAGE (GA-1a) antibody especially if there is a potential for commercial application.

Data and code availability

- Microarray data have been deposited at the GEO database and are publicly available as of the date of publication. Accession numbers are listed in the Key resources table.
- Unprocessed data, including uncropped western blots, microarray data and mass-spectrometry identifications used in this manuscript, have been deposited to Mendeley Data and are publicly available as of the date of publication. DOIs are listed in the Key resources table.

- The lead contact, upon request, will share ATAC-seq and ChIP-seq data reported in this paper.
- This paper does not contain original code.
- Any additional information required to reanalyze the data reported in this paper is available from the lead contact upon request.

EXPERIMENTAL MODEL AND SUBJECT DETAILS

Cell culture and generation IR-resistant cell lines

Cervical cancer cell lines HeLa and SiHa were obtained from the American Type Culture Collection. All cervical cancer cell lines are cultured in Dulbecco's Modified Eagle Medium (Sigma Aldrich) supplemented with 10% fetal bovine serum (FBS, Hyclone) in a humidified incubator at 37°C and 5% CO_2. Cell lines were authenticated via STR repeat assay performed by CTRAD. These cell lines were tested to be free of mycoplasma contamination by MycoAlert Mycoplasma Detection Kit (Lonza).

IR-resistant HeLa and SiHa cell lines were generated according to the protocol previously published by Kubo et al. (1982). Cells were seeded at a density of 500 000 cells in a 10-cm dish and allowed to attach overnight. Cells were then subjected to gamma irradiation at 1 Gray (1 Gy), a dose typically ascribed to patients with cervical cancer using the Biobeam 8000 irradiator, which uses a Caesium 137 radiation source. Media was changed for continued incubation on day six, and cells were re-plated 10 days post-irradiation. This comprises one cycle of radio-resistant cell generation. On day 14 of each cycle, the procedures mentioned above were repeated for the next cycle. IR-resistant lines received a total of five rounds of gamma irradiation.

Mice

Three to four-week-old female BALB/c nude mice were purchased from InViVos Pte. Ltd and housed and cared for throughout in specific pathogen-free (SPF) isolators according to the guidelines approved by IACUC (National University of Singapore).

METHOD DETAILS

Constructs, infection and transfection of human cell lines

GAGE expression lentiviral vector pLenti-CMV-f:G12 was generated by cloning the *GAGE12B* mRNA sequence (NM_001127345.1) into *Xba*I and SalI sites of the pLenti-CMV GFP-Puro (658-5) construct from Addgene. *GAGE12B* insert was PCR amplified from HeLa IR^R cDNA using the forward primer 5′-GCTCTAGAGCATGGACTACAAAGACGATGACGACAAGAGTTGGCGAGGAAGATCG ACCTA-3′ and reverse primer 5′-GGGTCGACTTAACACTGTGATTGCTTTTCACCTTCTTCAGGCG-3′. pLenti-CMV-f:G2/10 and pLenti-CMV-f:G13 constructs were generated by site-directed mutagenesis of the pLenti-CMV-f:G12 vector using the primers, forward primer 5′-GAAGATCGACCTATCGGCCTAGACCAAGG-3′ and reverse primer 5′-CCTTGG TCTAGGCCGATAGGTCGATCTTC -3′ to generate the TAT deletion and T-C mutations at position 109-112 of the *GAGE12B* mRNA sequence and forward primer 5′-CAAGGCGCTATGTAGAGCCTCCTGAAATG-3′ and reverse primer 5′-CATTTCAGGAGGCTCTACATAGCGCCTTG-3′ to generate the C to G mutation at position 136 of the *GAGE12B* mRNA sequence. Successful constructs were determined by Sanger Sequencing.

Lentiviral pMD.G envelope plasmid, dR8.91 package plasmid and pLenti-CMV-f:G12, 13 or 2/10 and pLenti-CMV-Empty (Mock) were transfected into HEK293FT cells at a final ratio 1:5:10. Lentiviral containing supernatant was collected, concentrated and introduced into HeLa P cells 3 days post-transfection. Forty-eight hours post-infection, puromycin was added to a final concentration of 1 μg/ml. Twenty-four hours after the addition of puromycin, surviving cells were trypsinised plated into 96-wells for single clone selection. Successful single clones were selected by western blotting for the presence of f:G12, f:G13 or f:G2/10. Successful clones were maintained in Dulbecco's Modified Eagle Medium (Sigma Aldrich) supplemented with 10% fetal bovine serum (FBS, Hyclone) and 1 μg/ml puromycin (Sigma Aldrich) in a humidified incubator at 37°C and 5% CO_2.

Xenograft models and microarray analysis

Three to four-week-old female nude mice were purchased from InViVos Pte. Ltd and housed and cared for throughout in specific pathogen-free (SPF) isolators according to the guidelines approved by IACUC (National University of Singapore). HeLa P, IR^R, HeLa-Mock or HeLa f:G12-OE (2.5×10^6) were mixed with an equal volume of Matrigel matrix (Corning®) and subcutaneously injected into the left flank of recipient mice. For microarray analysis, animals with a palpable tumor size of 1500 mm^3 were sacrificed by CO_2 euthanasia and tumor excised. Total RNA was extracted using TRIzol reagent (ThermoFisher Scientific, Cat. #15596018), following the manufacturer's protocol. RNA after purification were sent to the NUS Genomic Services Lab for the microarray experiment. The Illumina Human HT-12 v4 Expression BeadChip was adopted to conduct the microarray analysis. Each array contains more than 40,000 immobilized oligonucleotide probes with sequences derived from the National Center for Biotechnology Information Reference Sequence (NCBI RefSeq). Upregulated genes were identified as genes whose expression were increased by at least 2-fold compared to the parental cell lines identified for further validation by qPCR.

For IR treatment, animals with palpable tumor size of 120-150 mm^3 were treated with whole-body gamma irradiation using the Biobeam 8000 irradiator, which uses a Caesium 137 radiation source. Fractionated doses of 2 Gy each day were given for 3 days consecutively, followed by a 2-day break followed by another 2 Gy each day for another 3 consecutive days (total 12 Gy over

8 days). Weight and tumor size were measured by the Vernier calliper every alternate day. Tumor volume was calculated as [length (l) x width (w)^2] /2. Mice were sacrificed by CO_2 euthanasia, and tumors were excised 3 days after the last IR dose. All mice experiments were conducted under protocols approved by the Institutional Animal Care and Use Committee of the National University of Singapore.

qRT-PCR

Cells were lysed *in situ* on culture plates using TRIzol reagent (ThermoFisher Scientific, Cat. #15596018), following the manufacturer's protocol. One microgram of total RNA was converted to cDNA by using oligo(dT)20 primer according to the iScript Select cDNA synthesis kit manual (Bio-Rad). qPCR was performed using iTaq universal SYBR green supermix (Bio-Rad) with iQ5 Multicolor Real-time PCR detection system (Bio-Rad). pan-GAGE primers used in this study are forward: 5′-GAACCAGCAACTCAACGTCA-3′, reverse: 5′-TTCACCTCCTCTGGATTTGG-3′. *RPL13A* is used as an internal housekeeping control, and the primers used are forward: 5′-GGAGGTGCAGGTCCTGGTGC-3′, reverse: 5′-CAGGTACTTCAACTTGTTTCTGTAG-3′.

Clinical samples, RNA analysis and immunohistochemistry

Retrospective first biopsy formalin-fixed paraffin-embedded (FFPE) samples from 43 patients diagnosed with locally advanced cervical cancer between 2010-2015 and received standard radiotherapy at the National Cancer Institute of Singapore's Radiation Oncology Department were obtained from the National University Hospital Tissue Bank. The median follow-up period for these patients was 42 months. Of these 43 patients, 20 patients developed metastases (distant only OR local + distant metastases) and were classified as resistant. 23 patients remained disease-free at follow-up, and these were classified as sensitive. Immunohistochemistry (IHC) and pathology scoring were performed by a trained pathologist at the National University Hospital of Singapore's Department of Pathology. For IHC, the anti-GAGE12H (Thermofisher, Cat. #PA5-48611) was used at a dilution of 1:100. Antigen retrieval was performed at pH 5. GAGE levels within tumor cells were scored based on an intensity score range of 0-3 based on how intense the GAGE signal was within the tumor cells compared to unstained normal cells. As tumors are generally a heterogeneous population, the pathologist further looked at the percentage of tumor cells within each sample, which was GAGE positive, and gave each sample an extent score (Extent as 0, 1(1%–25%), 2 (26%–50%), 3 (51%–75%), 4 (76%–100%)). Multiplying the intensity by extent gave us an H-score.

For RNA analysis of FFPE samples, 10 μm sections were obtained and deparaffinized by xylene and subsequent hydration of tissue in decreasing ethanol concentrations. Hydrated tissue was lysed in TRIzol reagent (ThermoFisher Scientific, Cat. #15596018), following the manufacturer's protocol. cDNA synthesis and qRT-PCR of GAGE was performed as described in the previous section. Collection of clinical samples and use of patient material were conducted under protocols approved by the Ethics review board of the National University Hospital of Singapore.

For prospective studies, patients diagnosed with locally advanced cervical cancer and referred to the National Cancer Institute of Singapore's Radiation Oncology Department at the National University Hospital of Singapore were recruited. All patients received 28 fractions of external beam radiotherapy (EBRT) with concurrent weekly platinum-based chemotherapy followed by four brachytherapy fractions. Patients were classified as resistant if their tumor did not reduce by > 50% on clinical examination after completing concurrent chemo-radio-therapy (CRT). Diagnostic pre-treatment biopsy specimens and post-CRT second biopsy specimens were collected. Biopsy specimens were lysed in Trizol, and total RNA was isolated. GAGE expression was analyzed by qRT-PCR. This study was approved by the Ethics review board of the National University Hospital of Singapore. All samples were collected with informed consent from patients enrolled in this study.

2D viability and long-term colony formation assays

For viability assays, cells were seeded at 2000 cells per well in a 96-well plate and allowed to attach overnight. IR was performed the following day at varying doses using the Biobeam 8000 irradiator. Cell viability after irradiation was determined by crystal violet staining 72 hours post-IR.

For long-term colony formation assays, cells were seeded at 500 cells per well in a 24-well plate and allowed to attach overnight. IR was performed the following day with the Biobeam 8000 irradiator. Cell viability after irradiation was determined by crystal violet staining 14 days post-IR.

3D anchorage-independent and tumorsphere formation assays

For 3D anchorage-independent soft agar assays, 5000 cells suspended in DMEM were seeded in 0.7% top agar at a volume ratio of 1:1 (final agar concentration = 0.35%). One day after plating, top media was aspirated, and IR was performed the following day at 5 Gy using the Biobeam 8000 irradiator. Top media was replaced post-IR and changed every 3 days. Colony formation was assessed after 21 days. Colonies were stained using crystal violet, and sizes were measured using the Image-Pro Analyzer ver. 6.2. Colony diameters of at least 50 colonies from 3 biological replicates were collected and plotted as dot plots.

For tumorsphere formation assays in tumor-initiating media, cells were trypsinised from the 2D cultures and washed with PBS. After cell counting, they were resuspended in "tumour-initiating medium" [TIM; serum-free DMEM supplemented with 20 ng/ml human epidermal growth factor (EGF, Lonza CC- 4107), 20 ng/ml human basic fibroblastic growth factor (bFGF, Lonza CC-4068) and 2% v/v B27 Supplement (GIBCO, Cat. #12587010)]. The cell suspension was then passed through a 40 μm cell strainer and plated

onto UltraLow Attachment 96-well plates at a seeding density of 50 cells in 200 μL TIM per well. The cells were incubated at 37°C with 5% CO_2 for 14 days before spheres formed were stained with 2 μM calcein AM and 4 μM EthD-1 (Invitrogen). Dye solutions were prepared shortly before use and added directly into media without aspiration to avoid sphere loss and disintegration. One hour was given to allow dye penetration into the spheres before imaging with the Olympus IX81 inverted fluorescence microscope.

For viability post-irradiation, cells post-trypsinisation were plated at 50 cells per well in DMEM supplemented with 10% fetal bovine serum (FBS, Hyclone) in UltraLow Attachment 96-well plates. Cells were incubated at 37°C with 5% CO_2 overnight before they were subjected to IR using the Biobeam 8000 irradiator, which uses a Caesium 137 radiation source at 5 Gy. Cells were further incubated post-IR at 37°C with 5% CO_2 for 6 days and stained with 2 μM calcein AM and 4 μM EthD-1 (Invitrogen) and imaged as described above.

Generation of the pan-GAGE monoclonal antibody (GA-1a)

For the preparation of the antigen, the cDNA encoding for GAGE12 was sub-cloned from the pLenti-CMV-f:G12 into the pET28a vector to generate the pET28a-GAGE12-His vector for expressing histidine-tagged GAGE12 (GAGE12-His) in BL21(DE3) bacterial expression system. Protein expression was induced by adding 0.5 mM isopropyl β-D-1-thiogalactopyranoside in the culture medium at 16°C overnight. GAGE12-His was purified from the cell lysate using a HisTrap HP column (GE Healthcare) with a linear gradient of 10–250 mM imidazole in 20 mM sodium phosphate (pH 7.4) and 0.5 M NaCl.

The pan-GAGE monoclonal antibody (clone GA-1a) was generated in the laboratory of Dr. Shih-Chung Chang at the Department of Biochemical Science and Technology, National Taiwan University (NTU). The animal experiment was approved by the Institutional Animal Care and Use Committee of NTU (approval number: A201800006) and implemented in accordance with the animal care and ethics guidelines. The procedures for the generation of hybridomas were performed as described previously (Chiang et al., 2021). Briefly, BALB/c male mice were immunized three times at a 2-week interval through intraperitoneal injection with a mixture of 50 μg GAGE12-His and complete or incomplete Freund's adjuvant (Sigma-Aldrich), followed by a final booster injection of 25 μg GAGE12-His in PBS. For conducting the cell fusion experiment, Sp2/0 Ag14 cells were mixed with splenocytes derived from the donor mouse in the presence of 0.7 mL polyethene glycol 1500 (Sigma-Aldrich) at 37°C for 2 mins with gentle shaking, and 10 mL DMEM was then added to the cell mixture. After centrifugation, cells were resuspended in 30 mL DMEM containing 15% FBS (Hyclone), 1% penicillin-streptomycin, 1 mM sodium pyruvate (Thermo Fisher Scientific), and HAT Media Supplement (Sigma-Aldrich). Fusion cells (0.1 mL) were cultured in 96-well plates and grown at 37°C in the 5% CO_2 incubator. The culture media were collected for screening of the positive hybridoma clones by ELISA using 100 ng GAGE12-His as the antigen. The limiting dilution method was also applied for obtaining the single clone of the target antibody (clone GA-1a).

To purify the antibodies, the hybridoma cell culture media were filtered through a 0.45 μm membrane disc and then purified by the HiTrap Protein G HP column (GE Healthcare). The purified antibody was dissolved in PBS, and the concentration was determined by Bradford dye-binding method using mouse IgG as the standard. Antibody specificity was validated by western blotting with purified GAGE12 and GAGE2/10 proteins as well as in lysates obtained from cell lines expressing f:GAGE12 and GAGE2/10 proteins. Specificity for endogenous GAGE was validated in lysates obtained from HeLa Parental versus IR^R cell lines with and without GAGE knockdown.

Western blot analysis

Cells were lysed in modified RIPA buffer containing 50 mM Tris-HCl pH 7.4, 400 mM NaCl, 1% NP-40 0.25% sodium deoxycholate and 1 mM EDTA supplemented with protease and phosphatase inhibitors. Protein concentration was determined by Bradford assay. 2X Laemmli Sample buffer supplemented with 200 mM DTT was added at 1:1 ratio by volume, and lysates were heat-inactivated at 95°C for 3 mins. Equal amounts of protein were loaded for SDS-PAGE, and the signal was detected by the Western Lightning Plus-ECL detection system (Perkin Elmer). Image acquisition was performed using the Biorad ChemiDoc™ MP imaging system.

Antibodies used in this study were used at 1:1000 dilution unless otherwise stated and are as follows: anti-GAGE12B (Therma Fisher Scientific, Cat. #PA5-48149, 1:500), anti-pan-GAGE (clone GA-1a) (Dr.Shih-Chung Chang's Laboratory, National Taiwan University 1 μg/ml final concentration), anti-GAPDH (Santa Cruz Biotechnology, Cat. #sc-25778), anti-FLAG (Sigma Aldrich, Cat. #F3165), anti-α-tubulin (Santa Cruz Biotechnology, Cat. #sc-5286), anti-histone H3 (Cell Signaling Technologies-CST, Cat. #4499), anti-synemin/desmuslin (Santa Cruz Biotechnology, Cat. #sc-374484, 1:500), anti-Phospho-Histone H2A.X (Ser139) (CST, Cat. #9718), anti-H3K56Ac (CST, Cat. #4243), anti-H3K27Ac (CST, Cat. #4353), anti-H3K18Ac (CST, Cat. #13998), anti-H3K14Ac (CST, Cat. #7627), anti-H3K9Ac (CST, Cat. #9649), anti-H3K4Ac (Active Motif, Cat. #39381), anti-H4K12Ac (CST, Cat. #2591), anti-H4K8Ac (CST, Cat. #2594), anti-H4K5Ac (CST, Cat. #9672), anti-histone H4 (CST, Cat. #2935), anti-HDAC1 (CST, Cat. #5356), anti-HDAC2 (CST, Cat. #5113), anti-HDAC3 (CST, Cat. #3949), anti-HDAC8 (Upstate, Cat. #07-505), anti-p300 (Upstate, Cat. #05-257), anti-PCAF (CST, Cat. #3378), anti-β-actin (Sigma Aldrich, Cat. #A5316, 1:5000), PP2Ac (Upstate, Cat. #05-421), anti-pATM (Ser1981) (CST, Cat. #13050), anti-pChk2 (Thr68) (CST, Cat # 2197).

Immunofluorescence staining

Cells were fixed in 4% paraformaldehyde at room temperature for 30 mins. Permeabilization was performed using 0.5% Triton X-100 for 5 mins on ice. The primary antibody anti-FLAG (Sigma Aldrich, Cat. #F3165, 1:100) was used, and cells were stained at 4°C overnight, followed by staining with the Alexa Fluor chicken anti-mouse 488 antibody at room temperature (1:200) for 2 hours. Nuclei were stained with 1 μg/ml DAPI (Sigma Aldrich, Cat. #9542) for 10 mins. Staining was visualized using Fluorescence Microscopy.

Cellular fractionation

Cytosol, Nucleoplasm and Chromatin fractionation was performed as described by Chiu et al. (2014). To separate nucleoplasm and chromatin proteins, cells were lysed in lysis buffer (10 mM HEPES, pH 7.4, 10 mM KCl and 0.05% NP-40) on ice for 20 mins and then were centrifuged at 13,000 x g for 5 mins. The pellet was washed once with lysis buffer, resuspended in low salt buffer (10 mM Tris-HCL, pH 7.4, 2 mM $MgCl_2$ and 1% Triton X-100) and then incubated on ice for 15 mins. After centrifugation at 13,000 x g for 10 mins, the supernatant was saved as nucleoplasm fraction. The pellet was further resuspended in high-salt lysis buffer (20 mM Tris, pH 7.4, 500 mM NaCl and 0.5% NP-40) and incubated for 30 mins on ice with frequent vortexing. The supernatant was collected as chromatin fractions after centrifugation at 13,000 x g for 5 mins.

Mass spectrometry

Five hundred microgram of chromatin fraction isolated from Mock or f:12-OE cells as described above were diluted to a final NaCl concentration of 125 mM in 20 mM Tris, pH7.4 and 0.5% NP-40 containing buffer, and subjected to immunoprecipitation with anti-FLAG-antibody for 2 hours at room temperature using the Pierce Crosslink Immunoprecipitation Kit (Thermo Scientific, 26147) according to the manufacturer's protocol. Bound proteins were eluted into 1M Tris-CL, pH 9.5 to a final concentration of 100 mM immediately to neutralize the eluate for mass-spectrometry.

Immunoprecipitated protein from each sample was reduced in 4 mM DTT for 1 hour at 20°C, alkylated with 8 mM iodoacetamide for 1 hour at 20°C in the dark. Enzymatic digestion was performed first with Lys C (Wako) for 4 hours at 37°C (1:75), then with Trypsin for 16 hours at 37°C (1:75).

Digested peptides were next pre-fractionated on reverse-phase C18 stage tips in ammonium formate at pH 10. Each peptide fraction was then dried by vacuum centrifugation, reconstituted in 10% formic acid, and subjected to second dimension LC-MS at low pH. Samples were analyzed on an Orbitrap Q Exactive HFX spectrometer (Thermo Scientific) connected to a UHPLC 1290 system (Agilent). Raw files were processed using MaxQuant version 1.5.3.30 and the Andromeda search engine against the human Uniprot database (161042 entries, version Nov 2017).

Immunoprecipitation

One milligram of chromatin fraction isolated from Mock or f:12-OE cells as described above was diluted to a final NaCl concentration of 125 mM in 20 mM Tris, pH 7.5 and 0.5% NP-40 containing buffer, and subjected to immunoprecipitation with anti-FLAG-antibody or anti-SYMN-antibody. For total nuclear fractions, cells were first lysed in buffer containing 10 mM HEPES pH 7.4, 10 mM KCl and 0.05% NP-40. Incubate on ice for 20 mins and spun at 13000 g for 5 mins. The supernatant (cytosolic fraction) was removed. Pellets containing the nuclear fraction were lysed in modified RIPA containing 400 mM NaCl. One milligram of total nuclear fraction was diluted to a final NaCl concentration of 125 mM in 50 mM Tris, pH 7.4, 1% NP-40, 0.25% sodium deoxycholate, and 1 mM EDTA containing buffer and subjected to immunoprecipitation with anti-FLAG (2.5 μg), anti-SYMN (2.5 μg), anti-HDAC1 (1:100, CST) or anti-HDAC2 (1:100, CST) antibodies. The lysate was incubated with antibody at 4°C overnight with gentle rotation. TrueBlot Anti-Mouse Ig IP Agarose Beads (Rockland, Cat #00-8811-25) was then added, and the lysate was again incubated at 4°C with gentle rotation for two hours before elution with 2X Laemmli Sample buffer supplemented with 200 mM DTT. The lysate was heat-inactivated at 95°C for 3 mins.

Micrococcal Nuclease I (MNaseI) Digestion Assay

MNaseI digestion was carried out as described by Wang et al. (2012). Briefly, 1 X 10^6 cells were harvested and lysed in 200 μL HBN (15 mM Tris-HCl pH 7.6, 0.5 M sucrose, 60 mM KCl, 0,25 mM EDTA, 0.125 mM EGTA, 0.5% Triton X-100, 1 mM DTT and 0.5 mM PMSF). After 20 mins incubation on ice, nuclei were collected by centrifugation at 300 g for 5 mins. Nuclei was gently re-suspended in 50 μL nuclear buffer (20 mM Tris-HCl pH 7.6, 70 mM NaCl, 20 mM KCl, 5 mM $MgCl_2$ and 3 mM $CaCl_2$). Nuclei suspension was incubated with 0.06 to 0.5 units of MNaseI at 37°C for 10 mins. Digestion was terminated by the addition of EDTA and EGTA to a final concentration of 5 mM each. Nuclear pellets were collected by centrifugation at 6000 g for 5 mins and resuspended in 100 μL of lysis buffer (50 mM Tris-HCl pH 7.6, 100 mM NaCl, 5 mM EDTA, 0.5% SDS) supplemented with 200 μg/ml RNase A. After incubation at 37°C for 30 mins, 200 μg/ml Proteinase K was added and incubated further for 4 hours. Samples were purified using the ChIP DNA Clean and Concentrator Kit (Zymo Research) according to the manufacturer's protocol. DNA concentration was determined, and 250 μg of DNA per sample was resolved in 1.2% agarose gel.

Assay of Transposase Accessible Chromatin (ATAC) and Chromatin Immunoprecipitation (ChIP) sequencing

For ATAC-seq, 5 × 10^5 HeLa Mock or f:G12-OE cells were cryo frozen in fetal bovine serum containing 10% Dimethyl sulfoxide (DMSO). Cells were sent to NovogeneAIT Singapore for further processing for library preparation and sequencing.

For ChIP-seq experiments, 50 million f:G12-OE HeLa cells were cross-linked by adding formaldehyde (Sigma-Aldrich #252549) into the culture media at a final concentration of 1% for 10 mins at room temperature. The formaldehyde was then quenched by glycine (final concentration: 125 mM) at RT for 5 mins. Cells were rinsed three times with PBS and scraped off into a 15ml Falcon tube. Cell pellets were collected by centrifugation at 700 x g for 5 mins at 4°C. Cell pellet was then resuspended in 5 mL buffer 1 (50 mM HEPES-KOH pH 7.5, 140 mM NaCl, 1mM EDTA, 10% glycerol, 0.5% NP-40, 0.25% Triton X-100, supplemented by protease and phosphatase inhibitors) and mixed using a rotator (60 rpm) for 10 mins at 4°C. Cell suspension was then centrifuged at 1350 x g

for 5 mins at 4°C, and the pellet was resuspended in 5 mL buffer 2 (10 mM Tris-HCl pH 8.0, 200 mM NaCl, 1 mM EDTA, 0.5 mM EGTA, supplemented with protease and phosphatase inhibitors) followed by rotating-mixing (60 rpm, 10 mins, 4°C). The suspension was again centrifuged at 1350 x g for 5 min at 4°C; the pellet was resuspended 3.5 mL buffer 3 (10 mM Tris- HCl pH 8.0, 100 mM NaCl, 1 mM EDTA, 0.5 mM EGTA, 0.1% Na-Deoxycholate, 0.5% N-lauroylsarcosine, supplemented by protease and phosphatase inhibitors) and sonicated using the Qsonica 420-A probe at 80% amplitude, pulse 30 s, rest 30 s for 40 cycles to generate DNA fragments of around 500-100 bp. The sonicated lysate was mixed with 350 μL 10% Triton X-100, centrifuged at 20000 x g for 10 mins at 4°C and the supernatant was incubated with either 25 μL anti-FLAG® M2 Magnetic Beads-M8823 resuspended in 25 μL Buffer 3 or 10 μg anti-H3K56Ac antibody (Cat# 39281, Active Motif) at 4°C with constant rotation (60 rpm) overnight. H3K56Ac lysate-antibody complexes were then incubated with Protein G Agarose beads (30 μL slurry, Santa Cruz, for 2 hr) before washing. The immune complexes were washed with 1 mL buffer 4 (50 mM HEPES-KOH pH 7.5, 500 mM LiCl, 1 mM EDTA, 1.0% NP-40, 0.7% Na-Deoxycholate) 3 times, followed by one wash with 1 mL buffer 5 (10 mM Tris-HCl pH 8.0, 1 mM EDTA, 50 mM NaCl), and eluted by incubating the complexes with 250 μL elution buffer (50 mM Tris-HCl pH8.0, 10 mM EDTA, 1% SDS) for 15 mins. The eluates were then collected by centrifugation at 16000 x g for 1 min at room temperature. The eluates were reverse-crosslinked by incubation at 65°C overnight, mixed with 250 μL of buffer TE, and treated with RNase A (final concentration: 0.2 mg/ml, QIAGEN, #19101) at 37°C for 2 hr. The proteins in the immune complexes were removed by incubation with proteinase K (final concentration: 0.2 mg/ml, QIAGEN, #19131) at 55°C for 2 hr. ChIPed DNA was purified using the Zymo ChIP DNA Clean and Concentrator Kit (D8201). Purified DNA was sent to NovogeneAIT, Singapore, for library preparation and sequencing at 20 million reads.

ATAC-seq and ChIP-seq data was processed as follows. Raw reads were aligned to hg38 reference genome using bwa v0.7.13-r1126 aligner (Li and Durbin, 2009) followed by the removal of PCR duplicates with the Picard v2.28.0 markDuplicates utility (http://broadinstitute.github.io/picard/). Peaks were called using MACS2 v2.1.4 (Zhang et al., 2008) by extending reads to fragment size predicted by strand cross-correlation analysis from phantompeakqualtools v1.0 and parameter–nomodel (Landt et al., 2012). Intersection of peaks were identified using BEDtools suite (Quinlan and Hall, 2010).

Cell cycle analysis

For BrdU, Propidium Iodide (PI) double staining, cells were seeded at 2 × 10^5 cells per well in 6-well plates and incubated at 37°C and 5% CO_2 overnight. Cells were pulsed with 10 μM BrdU for one hour and fixed in 70% ethanol. Fixed cells were stained with anti-BrdU (3D4) Alexa Fluor® 647 at 4°C in the dark overnight. After incubations, cells were washed in 1X PBS and stained with PI for 30 mins at room temperature (50 μg/ml PI with 250 μg/ml RNase A in 1X PBS + 1% BSA 0.1% Triton-X). Cells were then washed and resuspended in 1 X PBS plus 1% BSA for analysis by Flow cytometry. Flow cytometry was performed using the Beckman Coulter CytoFLEX LX. Analysis was performed with CytExpert.

For PI time chase experiments, cells were seeded at 2 × 10^5 cells per well in 6-well plates and incubated at 37°C and 5% CO_2 overnight. Cells were subjected to IR at 5 Gy and harvested every 4 hours, and fixed in 70% ethanol. Cells were washed in 1X PBS and stained with PI for 30 mins at room temperature (50 μg/ml PI with 250 μg/ml RNase A in 1X PBS + 1% BSA and 0.1% Triton-X). Cells were then washed and resuspended in 1 X PBS plus 1% BSA for analysis by Flow cytometry. Flow cytometry was performed using the Beckman Coulter CytoFLEX LX. Analysis was performed with CytExpert.

In vitro HDAC and HAT Assay

In vitro, HDAC (Biovision, Cat. #K330-100) and HAT (Biovision, Cat. #K334-100) assays were performed according to the manufacturer's protocol. Briefly, cells were first lysed in buffer containing 10 mM HEPES pH 7.4, 10 mM KCl and 0.05% NP-40. Incubate on ice for 20 mins and spun at 13000 g for 5 mins. The supernatant (cytosolic fraction) was removed. The pellet containing the nuclear fraction was lysed in 100 mM NaCl RIPA, sonicated and incubated on ice with occasional vortexing for 20 mins. The lysate was precleared of cell debris by centrifugation at maximum speed for 20 mins. The supernatant was collected, and concentration was measured using Bradford. Ten micrograms of nuclear extract were used for each reaction to access either HDAC or HAT activity according to the manufacturer's protocol.

siRNAs and gene knockdown

Gene knockdown was performed using Lipofectamine RNAiMAX Transfection Reagent (Invitrogen) according to the manufacturer's protocol. Sequences of siRNAs used are as follows, siGAGE forward: 5′-CGAGGAAGAUCGACCUAUUdTdT-3′, reverse: 5′-AAUAG GUCGAUCUUCCUCGdTdT-3′, siSYNM forward: 5′-GGUUAGACCUGGAGGAGCUdT dT-3′, reverse: 5′-AGCUCCUCCAGGU CUAACCdTdT-3′, siHDAC1 forward: 5′- CAGCGACUGUUUGAGAACCdTdT-3′, reverse: 5′-GGUUCUCAAACAGUCGCUGdTdT-3′, siHDAC2 forward: 5′-UCCGUAAUGUUGCUCGAUGdTdT-3′, reverse: 5′-CAUCGAGCAACAUUACGGAdTdT-3′, siHDAC3 forward: 5′-GAUGCUGAACCAUGCACCUdTdT-3′, reverse: 5′-AGGUGCAUGGUUCAGCAUCdTdT-3′, siHDAC8 forward: 5′-GUCCCGAG UAUGUCAGUAUdTdT-3′, reverse: 5′- AUACUGACAUACUCGGGACdTdT-3′.

ATM inhibitor (KU60019) and Jasplakinolide treatment

ATM inhibitor KU60019 was purchased from Sigma Aldrich, Cat #SML1461. HeLa P and IR^R, as well as HeLa Mock and f:G12-OE cells, were subjected to 5 Gy of γ-irradiation in the presence or absence of 2.5 μM of ATMi (KU-60019) and cells were harvested for viability assay by crystal violet staining 72 hr post-treatment. For Jasplakinolide (Merck Millipore, Cat #420107) treatment,

Jasplakinolide was titrated in Mock and f:G12-OE HeLa cells to obtain IC20 at 72 hr. Mock and f:G12-OE HeLa cells were treated with IC20 dose for 24 hr followed by IR. Cell viability after Jasplakinolide treatment plus irradiation was determined by crystal violet staining 72 hours post-IR. HeLa f:G12-OE cells were treated with IC20 for 72 hr and subjected to cellular fractionation before western blotting analysis.

QUANTIFICATION AND STATISTICAL ANALYSIS

Experimental results were collected from three independent cultures for each sample. For clinical sample analysis, all individual expression data were obtained from each sample in each group and mean expression as a group was calculated. All data are analyzed with the GraphPad Prism 8.0 software. Data are shown as mean ± standard deviation (SD) in plots unless otherwise stated. Exact p values to the nearest four decimal points in group comparison, as derived from Student's two-sided t test unless otherwise stated, are indicated on the graphs. Statistical details of experiments can be found can be found in the figure legends.